AD-A107 718 UNIVERSITY OF SOUTHERN CALIFORNIA LOS ANGELES F/G 20/3
REACTIVE AND ENERGY TRANSFER PROCESSES OF THE NEUTRAL RADICAL S--ETC(U)
NOV 81 H HELVAJIAN, C WITTIG N00014-78-C-0585
UNCLASSIFIED NL

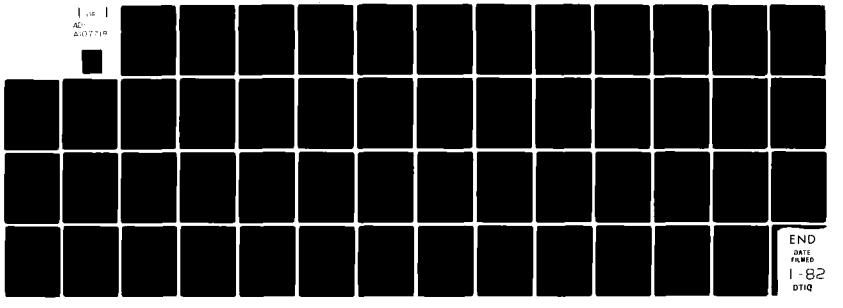

LEVEL I (12)

SECURITY CLASSIFICATION OF THIS PAGE (When Data Entered)

REPORT DOCUMENTATION PAGE

READ INSTRUCTIONS BEFORE COMPLETING FORM

1. REPORT NUMBER: N00014-78-C-0585	2. GOVT ACCESSION NO. AD A107718 / 3. RECIPIENT'S CATALOG NUMBER
4. TITLE (and Subtitle): REACTIVE AND ENERGY TRANSFER PROCESSES OF THE NEUTRAL RADICAL SPECIES HgBr IN GAS PHASE COLLISIONS	5. TYPE OF REPORT & PERIOD COVERED: Final Technical, May 1978 - May 1981 / 6. PERFORMING ORG. REPORT NUMBER
7. AUTHOR(s): H. Helvajian and C. Wittig	8. CONTRACT OR GRANT NUMBER(s): N00014-78-C-0585
9. PERFORMING ORGANIZATION NAME AND ADDRESS: Professor C. Wittig, SSC 403, University of Southern California, Los Angeles, CA 90007	10. PROGRAM ELEMENT, PROJECT, TASK AREA & WORK UNIT NUMBERS
11. CONTROLLING OFFICE NAME AND ADDRESS: Dr. H. Pilloff, Office of Naval Research, 800 N. Quincy, Arlington, VA 22217	12. REPORT DATE: November 5, 1981 / 13. NUMBER OF PAGES: 50
14. MONITORING AGENCY NAME & ADDRESS (if different from Controlling Office)	15. SECURITY CLASS. (of this report): Unclassified / 15a. DECLASSIFICATION DOWNGRADING SCHEDULE

16. DISTRIBUTION STATEMENT (of this Report)

Approved for public release; distribution unlimited.

17. DISTRIBUTION STATEMENT (of the abstract entered in Block 20, if different from Report)

Prepared for publication in J. Chem. Phys.

18. SUPPLEMENTARY NOTES

19. KEY WORDS (Continue on reverse side if necessary and identify by block number)

Lasers
Mercury monohalides
Mercury bromide
Harpoon mechanism

20. ABSTRACT (Continue on reverse side if necessary and identify by block number)

see reverse side

DD FORM 1 JAN 73 1473 EDITION OF 1 NOV 65 IS OBSOLETE
S/N 0102-LF-014-6601

Unclassified
SECURITY CLASSIFICATION OF THIS PAGE (When Data Entered)

Experimental investigations are conducted wherein kinetic process associated with the gas phase radical species HgBr are studied. These studies also serve to provide pertinent information to the development of the blue-green HgBr($B \rightarrow X$) laser. The experiments utilize laser induced fluorescence (LIF) and/or chemiluminescence as a means for observing the collisional behavior of HgBr radicals. Rate coefficients are measured for the quenching of electronically excited HgBr($B\,^2\Sigma^+_{1/2}$), vibrationally excited HgBr($X^2\Sigma^+_{1/2}$;v"), and the probability for energy transfer between metastable Hg(6^3P_0) atoms and HgBr($X^2\Sigma^+_{1/2}$). Various states of the radical are prepared either through photolysis of $HgBr_2$ yielding HgBr($B^2\Sigma^+_{1/2}$), or photolysis and subsequent spontaneous emission producing HgBr($X^2\Sigma^+_{1/2}$). Atomic excitation in mercury is via resonance absorption using 253.7 nm coherent radiation followed by spin orbit relaxation with N_2 buffer gas.

Various collisional partners ($HgBr_2$, CO, CO_2, O_2, H_2, Xe, N_2 and Br_2) were used to assess the electronic quenching of HgBr($B^2\Sigma^+_{1/2}$). The results show that Xe and N_2 are inefficient as quenchers ($\sim 10^{-13}$ $cm^3 molec^{-1} s^{-1}$) implying that both are suitable candidates as a buffer gas for the HgBr($B \rightarrow X$) laser. However, the other species have quenching rates which are orders of magnitude larger ($\sim 10^{-10}$ $cm^3 molec^{-1} s^{-1}$), these large quenching probabilities are attributed to reactive collisions or collision induced dissociation of HgBr. Using LIF, vibrational relaxation within the $X^2\Sigma^+_{1/2}$ manifold can be observed and quenching by the rare gases was found to be very efficient, specifically, rate coefficients measured for the quenching of v" states near v"+22, the lower laser level, was found to be gas kinetics. Furthermore, the quenching probabilities show a linear dependence with the C_6 parameter of the van der Waals interaction potential, implying that the magnitude of the quenching cross section is controlled by the long range attractive forces.

Measurements are also reported wherein Hg(6^3P_0) is deexcited by collisions with HgBr($X^2\Sigma^+_{1/2}$). The quenching rate coefficient is considerably larger ($(1.7 \pm 0.8) \times 10^{-9}$ $cm^3 molec^{-1} s^{-1}$) than the hard sphere collision rates and is consistent with ion-pair formation via the harpoon mechanism. The ion-pair produced correlates with the HgBr($B^2\Sigma^+_{1/2}$) product and provides a direct efficient pathway for channeling metastable Hg(6^3P_0) excitation into the upper laser state HgBr($B^2\Sigma^+_{1/2}$).

DISCLAIMER NOTICE

THIS DOCUMENT IS BEST QUALITY PRACTICABLE. THE COPY FURNISHED TO DTIC CONTAINED A SIGNIFICANT NUMBER OF PAGES WHICH DO NOT REPRODUCE LEGIBLY.

TABLE OF CONTENTS

ABSTRACT

Experimental investigations are conducted wherein kinetic process associated with the gas phase radical species HgBr are studied. These studies also serve to provide pertinent information to the development of the blue-green HgBr(B-->X) laser. The experiments utilize laser induced fluorescence (LIF) and/or chemiluminescence as a means for observing the collisional behavior of HgBr radicals. Rate coefficients are measured for the quenching of electronically excited $HgBr(B^2\Sigma^+_{1/2})$, vibrationally excited $HgBr(X^2\Sigma^+_{1/2},v'')$, and the probability for energy transfer between metastable $Hg(6^3P_0)$ atoms and $HgBr(X^2\Sigma^+_{1/2})$. Various states of the radical are prepared either through photolysis of $HgBr_2$ yielding $HgBr(B^2\Sigma^+_{1/2})$, or photolysis and subsequent spontaneous emission producing $HgBr(X^2\Sigma^+_{1/2})$. Atomic excitation in mercury is via resonance absorption using 253.7 nm coherent radiation followed by spin orbit relaxation with N_2 buffer gas.

Various collisional partners ($HgBr_2$, CO, CO_2, O_2, H_2, Xe, N_2 and Br_2) were used to assess the electronic quenching of $HgBr(B^2\Sigma^+_{1/2})$. The results show that Xe and H_2 are inefficient as quenchers ($\sim 10^{-13}$ $cm^3molec^{-1}s^{-1}$) implying that both are suitable candidates as a buffer gas for the HgBr(B→X) laser. However, the other species have quenching rates which are orders of magnitude larger ($\sim 10^{-10}$ $cm^3molec^{-1}s^{-1}$), these large quenching probabilities are attributed to reactive collisions or collision induced dissociation of HgBr. Using LIF, vibrational relaxation within the $X^2\Sigma^+_{1/2}$ manifold can be observed and quenching by the rare gases was found to be very efficient, specifically, rate coefficients measured for the quenching of v'' states near $v''=22$, the lower laser level, was found to be gas kinetic. Furthermore, the quenching probabilities show a linear dependence with the C_6 parameter of the van der Waals interaction potential, implying that the magnitude of the quenching cross section is controlled by the long range attractive forces.

Measurements are also reported wherein $Hg(6^3P_0)$ is deexcited by collisions with $HgBr(X^2\Sigma^+_{1/2})$. The quenching rate coefficient is considerably larger

($(1.7\pm0.8)\times10^{-9}$ $cm^3molec^{-1}s^{-1}$) than the hard sphere collision rates and is consistant with ion-pair formation via the harpoon mechanism. The ion-pair produced correlates with the $HgBr(B^2\Sigma^+_{1/2})$ product and provides a direct efficient pathway for channeling metastable $Hg(6^3P_0)$ excitation into the upper laser state $HgBr(B^2\Sigma^+_{1/2})$.

PREFACE

In this treatise, an effort has been made to investigate the kinetic processes associated with the radical species HgBr. In particular, experiments were designed to focus on the collisional behavior for the quenching of electronically excited HgBr(B) species, the deactivation of vibrationally excited $HgBr(X,v'')$ molecules, and the probability for energy transfer/reaction between metastable $Hg(6^3P_0)$ atoms and ground states HgBr(X) radicals. The experimental results provide data which are found to be pertinent to the development of the HgBr(B→X) laser and in general quite beneficial to the generic class of HgX lasers. Furthermore, these results are recast to add to the body of knowledge concerning interaction processes of simple free radicals.

The main body of the text consists of five chapters with the first primarily devoted to an introduction of the subject matter. The text also presents the relevant investigations to date and discusses those areas where further research is necessary. In Chapter II, experimental results are presented for the collisional deactivation of electronically excited HgBr(B) radicals. Rate coefficients for various collisional partners ($HgBr_2$, H_2, CO_2, CO, O_2, H_2, Xe, and Br_2) are measured and where appropriate, quenching mechanisms are discussed. Chapter III is devoted to measuring the collisional deactivation of vibrationally excited $HgBr(X,v'')$ species. Rate coefficients are measured for the deactivation of high vibrational states (v''-22) in $HgBr(X,v'')$; these v'' levels also serve as the ground state for HgBr(B→X) lasers. By using laser induced fluorescence at several wavelengths, the deactivation of $HgBr(X,v'')$ molecules through the entire $X^2\Sigma^+_{1/2}$ manifold can be monitored. In addition, the Absorbing-Sphere model with van der Waals interaction is presented as a possible scheme for describing the quenching mechanism.

The final experimental chapter (IV) discusses the possibility of energy transfer via chemical pumping of HgBr(X). Experimental results are presented for the deactivation rate of metastable $Hg(6^3P_0)$ atoms by HgBr(X). The results are discussed in light of correlation diagrams which show possible products and charge transfer theory which describes the reaction mechanism.

Finally, the discussion in Chapter V is presented for future investigation and Chapter VI contains a list of selected bibliography.

CHAPTER I

INTRODUCTION

For a number of years, there has been an interest in studying various gas phase processes associated with the free radical species HgX(X=Cl,Br,I). These diatomics were first observed nearly 100 years ago[1] but are once again the subject of active research, because they have been found to be potentially well suited to be the active species for an efficient high power laser.[2] Augmenting these laser studies, a host of other experiments have been done to elucidate some of the elementary physical and chemical processes of these radicals.[3] In this treatise, effort has been placed to provide some insight into these kinetic processes related specifically to the radical species HgBr.

The Simple Free Radical

It is perhaps wise to take the effort and acquaint the reader with a few concepts which would allow a more qualitative understanding of what there is to follow. It has been previously mentioned that HgBr is a free radical. Generally, all free radicals or radicals are transient species, in that they can be potentially reactive and usually are difficult to produce and study in the free state. They can be physically stable, meaning if undisturbed by collisions they do not spontaneously decompose.[4] Various methods have been used to produce radicals and observe them. Their spectra in emission has been observed in conventional flames (CH,C_2,OH),[5] atomic flames[6] where the interaction of atoms with molecules give the radical emission and through various chemical reactions.[7] They have been produced in electric discharges[8] (CH,C_2) or photolysis of stable parent molecules[9] (CH,NH,OH). Observing radicals in absorption is much more difficult, since the electronic states of the radical may not be well known and in any production scheme, one has to deal with other molecular fragments which may also absorb.

Chemical Kinetics: The Experimental Technique

It might also be fruitful to briefly address the subject of chemical kinetics, in the sense of it being a useful experimental technique for studying interaction processes on a macroscopic level. Broadly defined, chemical kinetics is the study of systems whose composition or energy distribution is changing with time. It compliments thermodynamics, in that thermodynamics allows one to predict the probability of a particular reaction taking place, while kinetics provides information on the reaction speed.[10-12] The two sciences differ in that for thermodynamics the equilibrium constant for a reaction is independent of the path leading reactants to products, while the kinetic rate of reaction is strictly dependent on the individual steps. In fact, the individual steps termed as the mechanism of the reaction is an important part of chemical kinetics. The use of kinetics as an experimental technique allows one, under certain controlled conditions, to use measured quantities which are not necessarily absolute but merely proportional to the quantity in the state. In measuring a particular reaction rate, it becomes the task to define the experiment as such, that its outcome reflects the evolution of the reaction under study in a simple manner. For instance, simple exponential behaviour is

easy to measure because it is not necessary to know the initial quantities and a semilog plot versus time will generate the system time constant. Characterization of some simple reaction systems utilized in this thesis are discussed below. The simple first order reaction where [A] and [B] are species concentrations and k the reaction rate is given as,[13]

$$[A] \longrightarrow [B] \tag{1}$$

$$-d[A]/dt = k[A] \tag{2}$$

$$[A] = [A]_0 e^{-kt} \tag{3}$$

Equation (2) is the differential rate expression and Equation (3) one simple solution. When the kinetic equation involves more than one reacting species, the integrated rate equations become complicated. In this case, if the experimental conditions lend themselves to it, it is possible to make an essential isolation of each of the reaction species by adjusting their concentrations so that one of them is present in considerable excess. In this case the concentration of the species present in excess will remain almost constant during the course of the reaction while the overall reaction order is experimentally reduced. A simple pseudo-first-order reaction is presented below.

$$[A] + [B] \longrightarrow [C] + [D] \tag{4}$$

$$-d[A]/dt = k[A][B] \tag{5}$$

If $[A]_0 = 20[B]_0$, then [A] essentially stays constant at the initial value of $[A]_0$ and,

$$-d[A]/dt = -d[B]/dt = k[A]_0[B] = k'[B] \tag{6}$$

$$[B] = [B]_0 e^{-k't} \tag{7}$$

Where again Equation (7) is the simple solution to the reaction in Equation (4). For consecutive type reactions where the intermediate concentration is under study, consider the following first-order reaction sequence.

$$[A] \longrightarrow [B] \tag{8}$$

$$[B] \longrightarrow [C] \tag{9}$$

$$-d[A]/dt = k_1[A] \tag{10}$$

$$-d[B]/dt = k_1[A] - k_2[B] \tag{11}$$

These first-order and first-degree differential equations can be solved by standard methods to yield,

$$[B] = \frac{[A]_0 k_1}{k_2 - k_1} (e^{-k_1 t} - e^{-k_2 t}) \tag{12}$$

Reducing k_1 and k_2 experimentally from a double exponential expression is always difficult to do, especially if k_1 is approximately equal to k_2. But if for some reason k_2 of Equation (9) is much greater than k_1 (Eq. (8)), for instance if species [B] is in a short lived state and it decays, changing character, then Equation (12) reduces to a sensible first-order reaction having the solution,

$$[B] = \frac{[A]_0 k_1}{k_2 - k_1} e^{-k_1 t} \tag{13}$$

The solution in Equation (13) now reflects the production of [B] (destruction of [A]) via reaction (6).

In retrospect it is perhaps important to briefly comment on the kinetics of radicals, that of HgBr. Because of their transient nature and potential for reactivity one can expect kinetic reaction rates to be very fast. Thus, it might be necessary to use measurement techniques which are responsive to fast time scales. Furthermore, these radicals (HgBr) do not exist freely but must be produced. The formation of these radicals from parent species also produces other product fragments which complicate both the experiment and kinetic analysis.

Historical Background

$HgBr_2$: The Parent Species for HgBr Radicals

One cannot begin to present a proper historical chronology of the mercury monohalides (HgX, X=Br,Cl,I) without first commenting on the historical background of the one prominent parent species HgX_2(X=Br,Cl,I). The emission produced by mercury dihalides in electric discharges was first observed 100 years ago by Pierce. The emission was resolved into discrete lines by Jones[14] and shortly thereafter by Lohnmeyer.[15] Twenty-five years later Wieland initiated his thirty year study (1929-1960) of the emission produced by discharge excitation of mercury di-halides. He showed that most of the emission lines arise from excited mercury monohalides (HgX, X=Cl,Br,I) and made detailed assignments, in particular, of the $B^2\Sigma^+_{1/2} \longrightarrow X^2\Sigma^+_{1/2}$ bands in HgX(Cl,Br,I).[16]

The study of photolytic pumping of mercury dihalides is also over fifty years old. In 1927, Terenin reported strong visible fluorescence when HgX_2(X=Cl,Br,I) was irradiated with ultraviolet light.[17] Specifically broad band blue emission (max - 505 nm)

was observed when $HgBr_2$ was irradiated between 190-210 nm. Terenin assigned the emission bands to HgBr, i.e. the photodissociation products were the electronically excited radical $HgBr(B^2\Sigma^+_{1/2})$ and a ground state halogen $Br(^2P)$ atom. (See Fig. I-1)

$$HgBr_2 \longrightarrow HgBr(B^2\Sigma^+_{1/2}) + Br(^2P_{3/2}) \quad (14)$$

$$HgBr(B^2\Sigma^+_{1/2}) \longrightarrow HgBr(X^2\Sigma^+_{1/2}) + h\nu \quad (15)$$

Terenin's conclusion had been predicted by Mulliken in 1925.[18] In 1932 Wieland reported a more thorough study of the photodissociation of $HgBr_2$.[19] His investigation on the absorption from 150 to 210 nm of the mercury dihalides revealed three broad continuum absorptions in $HgBr_2$. The absorption maxima were at 224 nm, 195 nm and 160 nm as well as a series of discrete bands near 183 nm. Excitation in the first band at 224 nm and in the discrete bands near 183 nm produced no fluorescence, while excitation in the bands at 195 nm and 160 nm produced emission between 505-350 nm and 270-250 nm, respectively. In 1938-1940 Wehrli reported higher resolution spectra of the discrete absorption bands in $HgBr_2$.[20] while Sponer and Teller interpreted the spectra by assigning the spectral terms to the ground and various excited states of $HgBr_2$.[21] Wadt in 1980

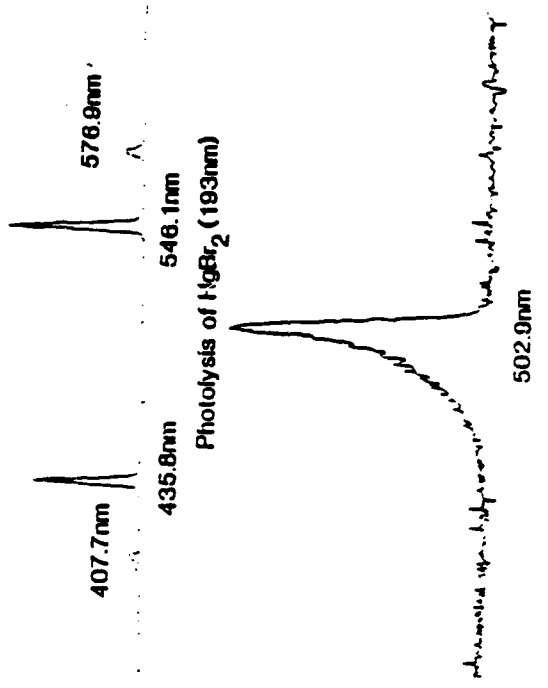

FIG. (I-1). Photolysis of $HgBr_2$ at 193 nm. The emission spectra is of $HgBr(B\rightarrow X)$ and was taken at 300 K, corresponding to a $HgBr_2$ density of $\sim 10^{13}$ cm^{-3}. The top spectra is the wavelength calibration, taken with a low pressure mercury lamp. Both spectra were taken using an optical multichannel analyzer (OMA).

investigated the electronic structure of $HgBr_2$ and its relationship to photodissociation.[22] Using theoretical calculations he assigned electronic spectral terms to the low-lying excited states of $HgBr_2$ and correlated them to various products using previous photodissociation experiments. The results are presented in Table (I-1).

With the advent of mercury monohalides as potential candidates for high power visible lasers,[23] there have been a flurry of investigations on both the decomposition of HgX_2(X=Cl,Br,I) and the efficient production of the excited radical $HgX(B^2\Sigma^+_{1/2})$. Maya for instance, has measured the absorption cross section of HgX_2(X=Cl,Br,I) in the ultraviolet. He finds the cross section at 193 nm is approximately $1x10^{-17}$ cm^2 for $HgBr_2$.[24] Wilcomb, in a later study, has made an absolute measurement of the efficiency for production of $HgBr(B^2\Sigma^+_{1/2})$ via photodissociation of $HgBr_2$ at 193 nm. He has determined the efficiency to be 0.95.[25] Zare in turn, has measured the electron impact cross section for HgX_2 to produce $HgX(B^2\Sigma^+_{1/2})$.[26] Specifically for $HgBr_2$, the cross section was measured to be $9.6x10^{-20}$ cm^2, showing that it is more efficient to produce $HgBr(B^2\Sigma^+_{1/2})$ from $HgBr_2$ via UV photolysis than electron

TABLE (I-1). $HgBr_2$ transition moments (%) and oscillator strengths (f) for the vertical dipole allowed excitations in $HgBr_2$. Also given are the calculated (experimental values given parenthetically) excitation energies (ΔE) of the various states (Reference (22)).

State	ΔE	λ(nm)	M	f	observed emission
$1^1\Sigma_g^+$	0.0[a]				
$1^1\Delta_g(1\pi_u \rightarrow 4\sigma_g)$	4.72(5.64)[b]	263	1.15	0.0239	none
$1^1\Sigma_u^+(2\pi_u \rightarrow 4\sigma_g)$	5.97(6.36)[b]	208	1.20	0.232	505-350nm
$2^3\Sigma_u^+(^2\pi_g \rightarrow 2\pi_u)$	6.33	159	0.471	0.00656	270-250nm

[a]Absolute energy is -70.50335 a.u from reference (22).
[b]Reference (29).

impact. There also have been investigations to obtain the rate constant for producing $HgBr(B^2\Sigma^+_{1/2})$ via dissociative excitation of $HgBr_2$ by rare gas metastable atoms and $N_2(A^3\Sigma_u^+)$.[27-28] The rate constants for $HgBr(B^2\Sigma^+_{1/2})$ formation from the excitation of $HgBr_2$ by $Xe(^3P_2)$ and $N_2(A\Sigma_u^+)$ was determined as $(5.3\pm1.5)\times10^{-10}$ $cm^3molec^{-1}s^{-1}$ and greater than $1\times10^{-10}cm^3molec^{-1}s^{-1}$ respectively.

Reactive Processes Which Yield HgBr

Rather than use the parent molecule HgX_2, people have sought to produce HgX radicals via reactive collisions of metastable mercury atoms $Hg(6^3P_{2,1,0})$ with halogen and halogenated hydrocarbon molecules.[30] With regards to the halogens, it was found that the cross section for reactive scattering (production of excited $HgBr(B^2\Sigma^+_{1/2})$ was approximately five times larger for the $^3P_2$ (5.4 eV) state of Hg than the $^3P_0$ (4.7 eV) state.[33] Bernstein, in a cross molecular beam chemiluminescene study, has placed the reactive cross section of $^3P_0$ Hg with Br_2 at approximately $3A^2$.[34] This observed spin-orbit dependence of the cross section perhaps implies a potential barrier in the $^3P_0$ reactive

channel, but not in the $^3P_2$. Of the halogenated hydrocarbons tested, the reaction of $CCl_4+Hg(^3P_2)$ has the highest cross section for producing $HgCl(B^2\Sigma^+_{1/2})$.[35]

Spectroscopy of HgBr

The spectroscopy of HgBr was first studied by Weiland in 1960 from his discharge emission studies on $HgBr_2$. He assigned vibrational transitions and their relative intensities for transitions between the $B^2\Sigma^+_{1/2}$ and $X^2\Sigma^+_{1/2}$ electronic states. Since then, it has been established that the ground state electronic configuration is $X^2\Sigma^+_{1/2}$.[36] Utilizing Weiland's results, Cool and Cheung calculated Franck-Condon factors and r-centroids for the B-->X transition in HgBr.[37] From Fig. (I-2) we see that the $X^2\Sigma^+_{1/2}$ state is bound by only 0.71 eV and correlates to ground state $Hg(^1S)$ and $Br(^2P)$ atoms. The next state above (X) is the repulsive $A^2\Pi$ which also correlates to ground state atomic species. The first bound state, termed $B^2\Sigma^+_{1/2}$, has a deep potential well (4.87 eV) and correlates to the ionic pair $Hg^+(^2S)$ and $Br^-(^1S)$. The most prominent feature of these potential energy curves is the relative displacement of the internuclear separation at the

FIG. (I-2). Potential energy curves for the (X),(A) and (B) states of $^{200}Hg^{79}Br$ without spin orbit coupling.

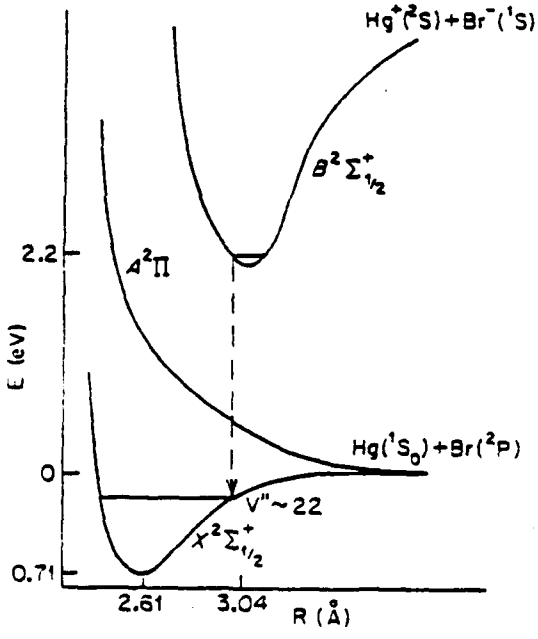

equilibrium point for the (B) and (X) states. Because of this unique character, the mercury mono-halides have been termed as excimer "like" molecules. Any Franck-Condon transitions from low vibrational levels of the (B) state end up at high vibrational levels of the ground (X) state, populations from these high vibrational levels can then be collisionally removed. Collisions with the excited molecule HgBr($B^2\Sigma^+_{1/2}$), hereafter as HgBr(B), will vibrationally relax the (B) electronic state manifold and further increase the population at low vibrational levels. This is apparent when studying the HgBr(B-->X) emission spectra (See Fig. (I-1), the prominent peak near 500 nm corresponds to transitions from low v' of the (B) state to high v" of the ground (X) state. Wadt has studied the electronic structure of HgBr, specifically the (X), (A), and (B) states.[38] He finds that as the internuclear distance decreases attractive ionic character begins to mix into the covalent (X) state while repulsive covalent character enters into the ionic (B) state. At the equilibrium separation for the (B) state (Re'), both (X) and (B) states are nearly 50-50 mixtures of covalent and ionic character, which maximizes the B-->X transition moment at (Re'). At the equilibrium of the (X) state, the (B) state is mostly (80%) covalent while the (X) state is mostly (80%) ionic. The introduction of spin orbit coupling in the calculations for HgBr (B) and (X) states has only a minor effect. Some of the effects are removing of the A state degeneracy, which splits into two states $A^2\Pi_{1/2}$, $A^2\Pi_{3/2}$ and the reduction of the (X) state dissociation energy to (0.33 eV). Wilcomb and Bernstein have calculated the $X^2\Sigma^+_{1/2}$ state dissociation energy from an analysis of vibrational level spacings using Wieland's spectroscopic data,[39] they claim that though their extrapolation is less secure for HgBr than HgI, the best estimate value is 0.74 eV. There have also been theoretical calculations for the HgBr(B-->X) radiative lifetime by Wadt (- 26.0 ns)[38] and by Duzy and Hyman (- 16 ns).[40] The latter study, not as detailed as the former calculations, used a physically intuitive charge transfer model in describing the B-- X transition. All the spectroscopic data for HgBr which have been gleaned from various sources are tabulated in Table (I-2).

TABLE (I-2). Spectroscopic constants for the (X), (B), (C), and (D) states of HgBr gleaned from various sources.

State	T_e(eV)	R_e(A)	ω_e(cm^{-1})	$x_e\omega_e$(cm^{-1})	B_e(cm^{-1})	α_e(cm^{-1})
$D^2\Pi_{3/2}$	4.78[a]		228.5[a]	0.950		
$C^2\Pi_{1/2}$						
$B^2\Sigma^+_{1/2}$	2.70[b] 2.91[a]	3.04[b] 3.10[c]	135.1[a]	0.29[b] 0.30[a]	0.032[b] 0.030[c]	0.00006[c] 0.00008[c]
$X^2\Sigma^+_{1/2}$		2.61[b] 2.62[c]	186.2[a]	0.97[a]	0.044[b] 0.043[c]	.00040[b] .00021[c]

State	D_e(eV)	μ(D)	M(D)	τ(B-->X)
$B^2\Sigma^+_{1/2}$	4.77[b],4.87[d]	5.51	3.88[b],4.12[e]	26.0[b],23.7[d]
$X^2\Sigma^+_{1/2}$	0.48[b],0.71[a]	2.62		

TABLE (I-2). (continued)

	Morse Parameters[c]		
State	$D_e(cm^{-1})$	$r_e(A)$	$\beta(A^{-1})$
$B^2\Sigma^+_{1/2}$	19,997.5	3.085	0.836
$X^2\Sigma^+_{1/2}$	6093.0cm^{-1}	2.6651	2.807

[a]Reference (36)

[b]Reference (38)

[c]Reference (37)

[d]Reference (44)

[e]Reference (45-46)

TABLE (I-3). Measured laser wavelengths for the mercury halide HgX(X=Cl,Br,I) $B^2\Sigma^+_{1/2} \rightarrow X^2\Sigma^+_{1/2}$ lasers.

Molecule	λ(air) in nm
HgBr[a]	502.0, 502.3, 502.6 503.9, 504.2, 504.6
HgCl[b]	552.0, 555.0 558.0, 559.0
HgI[b]	443.0, 444.0

[a]Reference (47)

[b]Reference (48)

HgBr(B→X) Lasers

As previously mentioned, the mercury monohalides have a large relative displacement of the (X) and (B) electronic states (see Fig. (I-2)), along with large (B→X) transition dipoles (see Table (I-2)). These fortuitous circumstances allow for population inversion and lasing action. Furthermore, under typical operating conditions, the excimer "like" nature of these radicals prevents bottlenecking of the lower laser level. Using various pumping schemes all the mercury halides HgX(X=Cl,Br,I) have been shown to lase on the $B^2\Sigma^+_{1/2} \rightarrow X^2\Sigma^+_{1/2}$ electronic transition.[41-43] Table (I-3) shows the observed lasing wavelengths for the various mercury halides. Since 1977, there has been research to obtain an efficient HgX(B→X) laser. This has prompted the design and building of HgX lasers using numerous excitation schemes. Since the upper laser level lifetimes are short (see Table (I-2) for HgBr), large excited state populations can only be obtained by intensive pumping schemes. HgX(B→X) lasing action has been achieved via excitation of HgX_2 or other compounds by UV photons (193 nm ArF laser, Xe_2^* emission at 172 nm), electrons (electron beam, UV preionized transverse electric discharge), and metastables (reactions with Hg^*, Xe^*, N_2^*). In the case of optial pumping (193 nm ArF laser photolysis of $HgBr_2$ vapor) lasing output was observed using both transverse and longitudinal excitation, with the transverse scheme giving higher gain.[47] To date, there have been more studies on the HgBr(B→X) laser than its counterparts HgCl and HgI. HgBr offers the advantage that the particular lasing wavelengths are well suited for underwater application in laser communications,[49] and it can be cleanly and efficiently produced using the high power ArF laser to photolyze $HgBr_2$. Output from the HgBr free running oscillator consists of several lines (see Table (I-3)), centered around two peaks at 502 and 504 nm. The lines are due to different rotational-vibrational transitions between the (B) and (X) states, with the added complexity caused by Br and Hg isotope shifts. In the main gain region, there is sufficiently fast interaction between the various states that from 495 to 505 nm, one effectively observes the behavior of a homogeneously broadened transition.[49] Thus, by injecting a narrow band signal into the HgBr oscillator, the laser output spectrum is condensed and locked to the injected signal. Single line operation of 0.05 nm width tunable between

495 and 505 nm, has been demonstrated with output energies equal to or exceeding that of the free-running oscillator.[50] Currently, HgBr/$HgBr_2$ dissociation lasers operate in pulsed mode with N_2 and He as buffer gases. The maximum laser output energies (9.8 J) has been obtained with an E beam sustained discharge with an overall efficiency of 1.8%.[51] Using a UV preionized discharge laser Schimitschek and Celto have studied the performance of the HgBr(B-->X) laser, deriving average values for the small signal gain g_0=6.6%/cm, the absorption coefficient a_0=0.35%/cm and the saturation flux I_{SAT}=200 KW/cm^2 for the case of when the buffer gas consists of 900 Torr He plus 100 torr N_2 as buffer gas.[52] From the average saturation flux, an estimate for the value of the stimulated cross section σ_{st} can be obtained.

$$\sigma_{st} = \frac{h\nu_1}{I_{SA}\ A_1^{-1}} \qquad (16)$$

For $h\nu_1$, the laser photon energy say at 500 nm, and the effective upper state lifetime A_1^{-1}=16 ns, one obtains a lower limit to σ_{st} as being $1.1x10^{-16}cm^2$. The Schimitschek laser can operate at a repetition rate of 100 Hz[53] with an overall efficiency of 0.95%. By changing

from a UV preionized discharge scheme to an X-ray preionizer (X-ray preionization is a convenient source of uniform ionization in large volume systems)[54-55], Fisher, et al. have measured an increase in overall efficiency to 1.4%.[56-57] So far a photolytically excited HgBr(B-->X) laser has operated in a sealed quartz cell for many thousand shots without any degradation in laser output.[58] This implies that for all practical purposes the $HgBr_2$ dissociation is completely reversible in that the net recombination rate is sufficiently large to keep from completely exhausting the $HgBr_2$ supply. In a separate experiment, Strauss et al., using kinetic absorption spectroscopy, have measured the dimerization of HgBr(X) (HgBr(X) + HgBr(X) --> products) with Ar as the third body buffer gas.[59] Although they could not precisely say whether the dimerization products were Hg_2Br_2 or $HgBr_2$+Br, their measured rate coefficient was ($2.0x10^{-11}cm^3molec^{-1}s^{-1}$). To date, no other recombination experiment has been done. The difficulties in the HgBr(B-->X) laser are 1) external heat is necessary to obtain large $HgBr_2$ vapor densities; though this problem is thought to be minor since in repetitively pulsed operation the excess heat generated by the discharge itself is more than enough to

supply the necessary heat;[53] 2) self absorption of the HgBr(B) radical at the laser wavelengths; the self absorption cross section has been calculated and is found to be 50 times smaller than that for stimulated emission; 3) electronic drive-circuit components, which is a common problem to all pulsed high power lasers; 4) the inherent low electron impact cross section for producing HgBr(B); 5) and the corrosive nature of the laser medium particularly with discharge electrodes. This is thought to be the major problem since side reactions of $HgBr_2$ and other dissociated products with metals can lead to undesired products which not only exhausts the $HgBr_2$ supply but also interferes with lasing action. Currently sealed devices with 316 stainless steel electrodes reach their half output power levels after 10^6 shots.[49] However, it is thought that the group of platinum metals is most likely to be compatible with the laser medium.[50]

HgBr Kinetics

Regardless of the excitation mechanism used, to obtain an efficient chemical laser is tantamount to understanding the collisional behavior of the active

species. Knowing the quenching kinetics is also essential in computer modeling of a chemical laser. For the mercury halide lasers there has been supportive research to measure quenching rate constants, but primarily for the destruction of the upper laser level HgBr(B). Rate coefficients have been measured using numerous collision partners, specifically those which might be likely candidates as buffer gases or possible halogen donor molecules. Table (I-4a,b,c) lists those rate coefficients measured to date. It was found that in general the rare gases had poor quenching cross sections,[32,61-64] while donor molecules i.e., for Br like HBr, CH_3Br, CCl_2Br_2, Br_2 and $HgBr_2$, had large cross sections.[32,61-61] Also, it was measured that Hg atoms generated from the photolysis of $HgBr_2$, if in large concentration will also quench HgBr(B).[62] Unlike the other strong quenchers N_2 was seen to be a poor quenching partner for all HgX(B) species.[61-64] Further studies to experimentally establish the HgBr(B-->X) radiative lifetime have also been done. Using the sensitive technique of laser induced fluorescence Djeu and Haxaa have measured the lifetime for HgBr(B) to be 23.2 ns;[45] Wagnant and Eden in a separate experiment measured 23.7±1.5 ns[46] in agreement with the previous

TABLE (I-4a). Quenching rate constants for HgCl($B^2\Sigma^+_{1/2}$); k_Q($cm^3 molec^{-1} sec^{-1}$) and τ(B—>X) = 22.2 ns.[a]

Q	Mandle et.al.[a]	Tang et.al[b]
He	4.1×10^{-14}	
Ne	3.3×10^{-14}	
Ar	5.0×10^{-14}	$<1.5\times10^{-13}$
Kr	7.3×10^{-14}	
Xe	3.1×10^{-14}	
N_2	6.2×10^{-14}	
Cl_2	1.7×10^{-10}	5.7×10^{-10}
HCl	1.1×10^{-10}	
CCl_4	1.6×10^{-10}	

[a]Reference (61)
[b]Reference (32)

TABLE (I-4b). Quenching rate constants for HgBr($B^2\Sigma^+_{1/2}$); k_Q($cm^3 molec^{-1} sec^{-1}$) and τ(B—>X) = 23.2 ns.[d]

Q	Mandle et.al.[a]	Eden et.al.[b]	Bazhulin et.al.[c]
He	$<6.4\times10^{-14}$	$<5.0\times10^{-13}$	5.6×10^{-14}
Ne		5.3×10^{-13}	
Ar	$<6.4\times10^{-14}$	7.4×10^{-13}	
Xe	3.0×10^{-13}	3.7×10^{-12}	6.0×10^{-13}
N_2	$<6.4\times10^{-14}$	4.4×10^{-12}	2.3×10^{-13}
Hg		1.3×10^{-10}	
Br_2	2.9×10^{-10}	5.5×10^{-10}	
HBr	1.3×10^{-10}	2.0×10^{-10}	
CH_3Br		3.9×10^{-10}	
CCl_2Br_2		4.3×10^{-10}	
CCl_3Br	1.8×10^{-10}		
CF_3Br	8.7×10^{-10}		
$HgBr_2$		1.7×10^{-10}	

[a]Reference (61)
[b]Reference (62)
[c]Reference (63)
[d]Reference (45)

TABLE (I-4c). Quenching constants for HgI($B^2\Sigma^+_{1/2}$) k_Q ($cm^3 molec^{-1} sec^{-1}$) and τ(B—>X) = 27.3 ns.

Q	Rokio et.al.[a]	Eden et.al.[b]
He	$<2.9\times10^{-14}$	
Ne	$<2.9\times10^{-14}$	
Ar	1.1×10^{-13}	3.3×10^{-13}
Xe	2.2×10^{-13}	7.1×10^{-13}
N_2	$<2.9\times10^{-14}$	1.1×10^{-12}
CF_3I	2.9×10^{-10}	2.9×10^{-10}
I_2	$<1.1\times10^{-8}$	
HI		1.0×10^{-10}
Hg		$\leq 3.0\times10^{-1}$
HgI_2		3.6×10^{-10}

[a]Reference (64)
[b]Reference (62)
[c]Reference (45)

study but both studies being in slight contradiction with theoretical calculations.[40]

Shortcomings Of HgBr Kinetic Studies

Although there have been a large number of experiments investigating various processes associated with the HgX species, most recent studies have been strictly concerned with those aspects which are only germane to the HgX(B—>X) laser. This has been specially true in the kinetic studies of the HgX(X=Cl,Br,I) radical. A large portion of the available kinetic data describes the collisional behavior of the excited HgX($B^2\Sigma^+_{1/2}$) radical. Furthermore in these studies, little effort was placed in understanding those collisional processes which provide much needed information concerning the kinetics of electronically excited radicals. Also there has not been an investigation to measure rates of removal of population from the lower laser levels (HgX($X^2\Sigma^+_{1/2}$, v'')). It is important to measure such rates and insure that collisional quenching can be made sufficiently large to overcome pumping rates and thus prevent laser self termination from population

bottlenecking. Also, it is necessary to find specifically those species which quench the lower laser level but do not deactivate the upper laser state. Furthermore, it could be of interest to both physical chemists and laser research scientists to study reactive processes with the ground state HgX($X^2\Sigma^+_{1/2}$) radical with the possibility of producing electronically excited molecules, i.e. HgX($B^2\Sigma^+_{1/2}$). The study of such processes not only provides the possible means of chemically pumping the HgX(B—>X) laser, but advances such knowledge of energy transfer in transient radical species.

Investigations Of This Treatise

In this treatise, effort has been placed to investigate those shortcomings previously mentioned for the specific case of the radical species HgBr. It is hoped that by examining such kinetic processes for HgBr, any general results which are obtained could also be applied to the generic class of mercury mono-halides. Furthermore, these results not only serve to obtain pertinent information for the class of HgX(B—>X) lasers, but they are also recast, to elucidate some

aspects of the elementary physical and chemical processes of such species.

References (Chapter I)

[1]B.O. Peirce, Wied. Ann. 6, 597 (1879).

[2]C.K. Rhodes, ed., Excimer Lasers (Springer-Verlag, Berlin, 1979).

[3]J. Maya, IEEE J. Quantum Electron. QE-15, 579 (1979).

[4]G. Herzberg, The Spectra and Structure of Simple Free Radicals (Cornell University Press, Ithaca, 1971).

[5]E.M. Sulewicz, P.J. Padley, R.E. Smith, Proc. Roy. Soc. A 125, 129 (1970).

[6]M. Polanyi, Atomic Reactions (Williams and Norgate, London, 1932).

[7]A.G. Gaydon, Spectroscopy and Combustion Theory (Chapman & Hall, London, 1942).

[8]B.A. Thrush, Chem. Brit. 2, 287 (1966).

[9]D.A. Ramsay, J. Chem. Phys. 21, 960 (1953).

[10]S.W. Benson, The Foundations of Chemical Kinetics (McGraw-Hill, New York, 1960).

[11]R.E. Weston, Jr., H.A. Schwarz, Chemical Kinetics (Prentice-Hall Inc., New Jersey, 1972).

[12]A.A. Frost, R.G. Pearson, Kinetics and Mechanism 2nd ed. (John Wiley & Sons, Inc., New York, 1961).

[13]An exhaustive study on kinetics can be found in References 10-12.

[14]A.C. Jones, Wied. Ann. 62, 30 (1897).

[15]J. Lohnmeyer, Z. Wiss. Photogr. 4, 367 (1904).

[16]H. Wieland, Helv. Phys. Acta 2, 46 (1929); 14, 420 (1941); Z. Elektrochem. 64, 761 (1960).

[17]A. Terenin, Z. Phys. 44, 713 (1927).

[18]R.S. Mulliken, Phys. Rev. 26, 1 (1925).

[19]H. Wieland, Z. Phys. 76, 801 (1932); 77, 157 (1932).

[20]M. Wehrli, Helv. Phys. Acta 11, 339 (1938).

[21]E. Sponer, E. Teller, Rev. Mod. Phys. 13, 75 (1941).

[22]W.R. Wadt, J. Chem. Phys. 73, 2469 (1980).

[23]J.H. Parks, Appl. Phys. Lett. 31, 192 (1977); 31, 297 (1977).

[24]J. Maya, J. Chem. Phys. 67, 4976 (1977).

[25]B.E. Wilcomb, R. Burnham, N. Djeu, Chem. Phys. Lett. 75, 239 (1980).

[26]J. Allison, R.N. Zare, Chem. Phys. 13, 263 (1978).

[27]R.S.F. Chang, R. Burnham, Appl. Phys. Lett. 36, 397 (1980).

[28]D.W. Fahey, L.D. Schearer, J. Chem. Phys. 72, 6318 (1980).

[29]H. Wieland, Z. Phys. 76, 801 (1932).

[30]T. Shay, B. Hammatt, T. Stermitz, G.J. Collins, J. Chem. Phys. 72, 1635 (1980).

[31]F.J. Wodarczyike, A.B. Harker, (unpublished).

[32]K.Y. Tang, R.O. Hunter, Jr., J. Oldenettel, D.L. Huestis, J. Chem. Phys. 70, 1492 (1979).

[33]R.F. Krause, S.G. Johnson, S. Datz, F.E. Schmidt-Bleek, Chem. Phys. Lett. 11, 577 (1975).

[34]S. Hayashi, T.M. Mayer, R.B. Bernstein, Chem. Phys. Lett. 51, 419 (1978).

[35]Op. cit. (reference 33).

[36]K.P. Huber, G. Herzberg, Molecular Spectra and Molecular Structure: Constants of Diatomic Molecules (Van Nostrand, New York, 1979).

[37]Hai-Ho Cheung, T.A. Cool, J. Quant. Spectrosc. Radiat. Transfer 21, 197 (1979).

[38]W.R. Wadt, Appl. Phys. Lett. 14, 658 (1979).

[39]B.E. Wilcomb, R.B. Bernstein, J. Molec. Spectrosc. 62, 442 (1976).

[40]C.Dusy, H.A. Hyman, Chem. Phys. Lett. 52, 345 (1977).

[41]W.T. Whitney, Appl. Phys. Lett. 12, 239 (1978).

[42]J.G. Eden, Appl. Phys. Lett. 11, 448 (1977).

[43]J.G. Eden, Appl. Phys. Lett. 11, 495 (1978).

[44]B. Rosen, Spectroscopic Data Relative to Diatomic Molecules (Pergamon Press, New York, 1970).

[45]N. Djeu, C. Mazza, Chem. Phys. Lett. 46, 172 (1977).

[46]R.W. Waynant, J.G. Eden, Appl. Phys. Lett. 11, 708 (1978).

[47]E.J. Schimetschek, J.E. Celto, J.A. Trias, Appl. Phys. Lett. 11, 608 (1977).

[48]R. Burnham, Appl. Phys. Lett. 11, 156 (1978).

[49]R. Burnham, E.J. Schimetschek, Laser Focus June (1981).

[50]T.M. Shay, F. Hanson, D. Cookin, presented CLEO '81, June 10-12, 1981, Washington (unpublished).

[51]J. Reis et.al., Avco Everett Research Laboratory Inc. (unpublished).

[52]E.J. Schimitschek, J.E. Celto, Appl. Phys. Lett. 16, 176 (1980).

[53]J.E. Celto, E.J. Schimitschek (unpublished).

[54]S.C. Lin, J.I. Levatter, Appl. Phys. Lett. 34, 505 (1979).

[55]S. Watanabe et.al., Appl. Phys. Lett. 18, 3 (1981).

[56]C.H. Fisher et.al., Proceedings, Lasers '80, 1980, New Orleans (unpublished).

[57]C.H. Fisher et.al., Mathematical Sciences Northwest Inc. (unpublished).

[58]E.J. Schimitschek, Proceedings, Electro-Optic/Lasers '79, 1979, Los Angeles (unpublished).

[59]G. Greig, H.E. Gunning, O.P. Strausz, J. Chem. Phys. 52, 3684 (1970).

[60]C.S. Liu et.al., in Proceedings, Lasers '80, Dec. 1980, New Orleans (unpublished).

[61]A. Mandl, J.H. Parks, C. Rozlo, J. Chem. Phys. 72, 504 (1980).

[62]J.G. Eden, R.W. Waynant, Appl. Phys. Lett. 14, 324 (1979).

[63]S.P. Bashulin, N.G. Basov, V.S. Zuyev, Yu.S. Leonov, Yu.Yu. Stoilov, Kvantovaya Elektron (Moscow) 5, 684 (1978).

[64]C. Rozlo, A. Mandl, J. Chem. Phys. 72, 541 (1980).

CHAPTER II

ELECTRONIC QUENCHING OF HgBr($B^2\Sigma^+_{1/2}$)

Introduction

The HgBr($B^2\Sigma^+_{1/2}$) radical, hereafter referred to as HgBr(B) can be efficiently produced by optical excitation of $HgBr_2$ at wavelengths near 190 nm.[1] These excited species have a short natural lifetime (~ 23 ns)[2] and can quickly decay to the ground $X^2\Sigma^+_{1/2}$ electronic state producing a broad band emission spectra.[3] HgBr(B-->X) spectra is in the visible wavelengths with a prominent peak near 500 nm (see Fig. (II-1)). The spectra is also nearly devoid of all vibrational and rotational structure, which is attributed to the overlapping of closely spaced rotational and vibrational states[4] along with the numerous isotope shifts. Experiments which involve the HgBr($B^2\Sigma^+_{1/2}$) state can benefit by the fact that 1) the short natural lifetime can simplify collisional quenching studies, usually the deactivation by trace impurities become negligible and only those species in great abundance dominate the

deactivation kinetics; 2) the B—>X transition allows the convenience of using visible detection apparatus which normally have high gain and are responsive to short transient signals. Obviously all collisional processes involving the $D^2\Sigma^+_{1/2}$ state of HgBr are pertinent to the development of HgBr(B—>X) lasers but in addition, such processes are of fundamental importance, as they provide information concerning the kinetics of an electronically excited free radical. Collisional quenching of the $B^2\Sigma^+_{1/2}$ state can proceed via chemical reaction, collision induced dissociation, or deexcitation to the $X^2\Sigma^+_{1/2}$ state. In this chapter, experimental results are presented for quenching of HgBr(B) by various small molecules. The results show some amazing differences between quenching species which are similar in most respects (e.g. CO and O_2 are very efficient quenchers and N_2 is an inefficient quencher).

Experimental

The experimental arrangement is shown schematically in Fig. (II-1). Briefly, the output from an ArF laser (Lumonics, 193 nm, 80-100 mJ, 20 nsec FWHM (see Fig. (II-2)) is sent into a screen room and into a

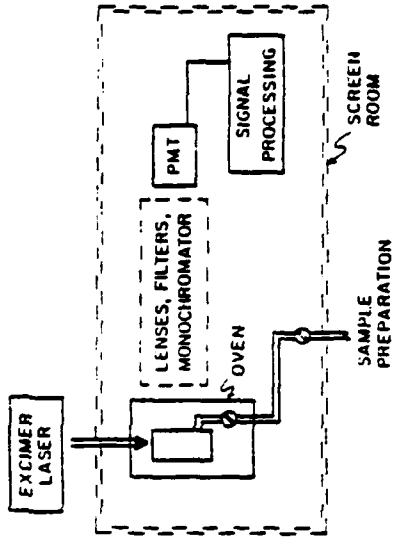

FIG. (II-1). Schematic drawing of experimental arrangement.

FIG. (II-2). Enlarged photograph trace taken from a CRT depicting the ArF laser output pulse duration. The power supply voltage was set at 35 KV (18.6 J stored energy).

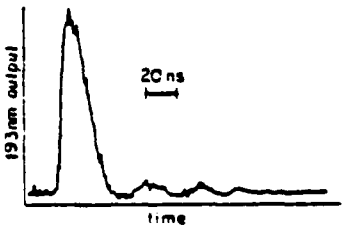

FIG. (II-3). Typical data from the transient digitizer/signal averager combination. The HgBr(B) fluorescence signal is digitized at 10 ns intervals. The origin of the time scale is nearly coincident with the termination of the ArF laser pulse (40-50ns duration). The data was taken with 950 mTorr of $HgBr_2$ in the cell.

fluorescence cell which contains the sample under consideration. Fluorescence is observed at right angles to the laser beam with a PMT (RCA 8575, 260-880 nm, 3 nsec) and spectral resolution is accomplished either with filters or a 0.75 m monochromator (Jarrel-Ash). Since the signals from the PMT were very large, great care was taken to insure that the PMT was operating in the linear regime. The signals were recorded by (1) photographing the signal directly using a fast oscilloscope, (2) digitizing the signal with a fast transient digitizer (Tektronix 7912), or (3) digitizing and averaging the signal with a slower transient digitizer/signal averager combination (Biomation & Tracor Northern, 10 ns gate). After using each method, it was found that (3) is the most convenient and reliable. Signals were recorded only after the termination of the ArF laser pulse where the fluorescence decay could be described by a single exponential over several lifetimes (Fig. (II-3)). To insure that the ArF laser pulse did not contain long-tails, a separate small experiment was conducted where the fluorescence from an ArF pumped Coumarin Dye (EXCITON C500) was monitored using a fast oscilloscope. A tracing of a photograph of the oscilloscope scan is

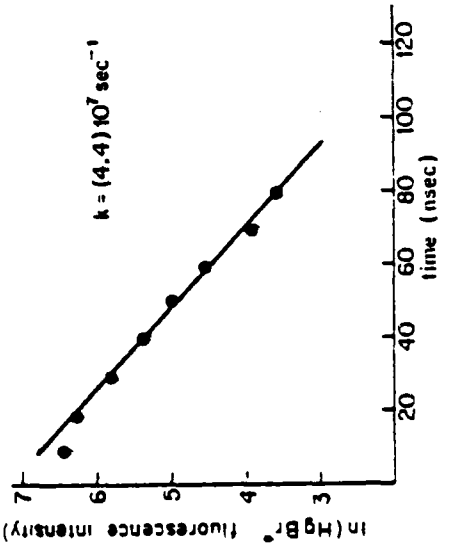

shown in Fig. (II-2).

$HgBr_2$ is a powder at room temperature, but has a reasonable vapor pressure at modest temperatures (100 mTorr at 373 K).[5] In Table (II-1), an extensive $HgBr_2$ vapor pressure data is tabulated. These data for temperatures lower than 409 K are extrapolated using computer least square fitting with known parameters.[5] The fluorescence cell is constructed from quartz and is contained inside a commercial oven (Trans Temp Co.). Fluorescence is observed through the partially transparent (thin Au coating on quartz) walls of the oven. By controlling the oven temperature, one is able to establish the $HgBr_2$ concentration during the course of an experiment. To insure that $HgBr_2$ solid is not present in the region of laser photolysis, the main body of the fluorescence cell is kept 10-15°C warmer than the side arm. The cell has Suprasil windows, to allow passing of 193 nm, and is connected to the vacuum system with a stopcock which uses a glass to glass seal. Since the stopcock is also housed inside the oven, this seal insures that those contaminants which usually outgas from normal O ring seals will be absent. Nominally, the cell is maintained near 378 K, which provides an $HgBr_2$ density of $3.6 \times 10^{15} cm^{-3}$. At this density of

TABLE (II-1). $HgBr_2$ vapor pressure data tabulated using computer least squares fitting (parameters are from Reference (5)).

T(°C)	Vapor Pressure (Torr)	T(°C)	Vapor Pressure (Torr)
200	24.76	160	3.92
196	20.96	156	3.18
192	17.63	152	2.57
188	14.85	148	2.06
184	12.44	144	1.64
180	10.37	140	1.30
176	8.61	136.5	1.00
172	7.12	132	0.90
168	5.87	128	0.71
164	4.81	124	0.55

TABLE (II-1). (continued)

T(°C)	Vapor Pressure (Torr)	T(°C)	Vapor Pressure (mTorr)
120	0.43	80	18.10
116	0.33	76	12.13
112	0.25	72	7.95
108	0.18	68	5.09
104	0.14	64	3.17
100	0.103	60	1.91
96	0.07507	56	1.17
92	0.05386	52	0.63
88	0.03807		
84	0.02648		

parent species, quenching of HgBr(B) by undissociated parent molecules or photofragments contributes only a very small amount to the observed quenching (average gas kinetic collision rates are 10 collision/usec-Torr;[6] for HgBr(B), A^{-1} - 23 ns and at a pressure of .1 Torr, results in a collision rate of 0.023 collisions in one lifetime).

Chemicals were purified as follows. $HgBr_2$ (Baker Analyzed Reagent grade) was pumped on at temperatures up to 100°C in order to remove volatile compounds (largest impurity $HgCl_2$ 0.2%). Br_2 (Baker Analyzed Reagent 99.9% min) was subjected to repeated distillation from 263 to 77 K and slow passage over P_2O_5. In addition, the apparatus in which the Br_2 was to be used was seasoned by exposure to Br_2, and heated under vacuum as much as possible in order to minimize the amount of H_2O on the surfaces. N_2 and Xe were research grade (Airco, 99.99% min) and were used without further purification. Other gases were typically 99.9% pure and were also used without further purification. Since the rate coefficients for these species were very large ($\geq$ 0.1 gas kinetic), effects due to impurities are minimal.

Results

The processes of concern are written in the following equations.

$$HgBr_2 + h\nu(193\ nm) \longrightarrow HgBr(B) + Br(^2P) \quad (1)$$

$$HgBr(B) \longrightarrow HgBr(X) + h\nu \quad (2)$$

$$HgBr(B) + M \longrightarrow \text{products} \quad (3)$$

where M are the quenching species. The quenching species have very small absorption cross sections at 193 nm[7-9] and therefore one need not be concerned about excitation and possible dissociation of the quenching species. A comment has to be made on the possible absorption of 193 nm radiation by newly formed HgBr(B) and HgBr(X) radicals. For instance, if the ArF intensity is high enough, those HgBr(B) which formed in the leading edge of the ArF laser pulse and which have not yet decayed can absorb a second 193 nm photon to form excited atomic states of Hg and Br.[10] Furthermore, any HgBr(X) could also absorb one or two UV photons and form numerous excited product species.[10] An indication of the one photon dissociation of HgBr(X) molecule is the 253.7 nm emission from Hg $6^3P_1 - {}^1S_0$ transition, while a two photon dissociation leads to higher excited

state of Hg such a 7^3S_1. Population in the 7^3S_1 state can be detected via the Hg $7^3S_1 - 6^3P_1$, transition at 435.8 nm.[11] Using appropriate narrow band filters no such emission was detected. This affirms that the density of electronically excited Hg atoms is small and that atoms formed from the multiphoton dissociation of HgBr will have negligible quenching effect. The rate equation describing (1) - (3) is

$$-d[HgBr(b)]/dt = A[HgBr(B)] + \sum k_M[M][HgBr(B)] \quad (4)$$

where A is the Einstein coefficient for the B$\longrightarrow$X transition ($A=4.3\times10^7 s^{-1}$), and k_M is the quenching rate coefficient for species M. With the termination of the ArF laser, (4) has the trivial solution of exponential decay with a lifetime given by

$$k = A + \sum k_M[M] \quad (5)$$

By varying [M], one can obtain k_M and A. As mentioned above, quenching by undissociated parent molecules is insignificant, contributing only 1% (at 100 mTorr, $(k'[HgBr(B)])/A \approx 0.01$; where k' is the quenching rate by $HgBr_2$) to the overall quenching. Typical data are shown in Fig. (II-4), and the results of the measurements are summarized in Table (II-2). The

FIG. (II-4). A least squares fit of the dependence of the fluorescence decay rate on pressure for O_2 and H_2. Each point represents an average of 200 fluorescence traces. N_2, whose quenching rate coefficient can only be measured at much higher concentrations than those shown in the figure, is shown for comparison.

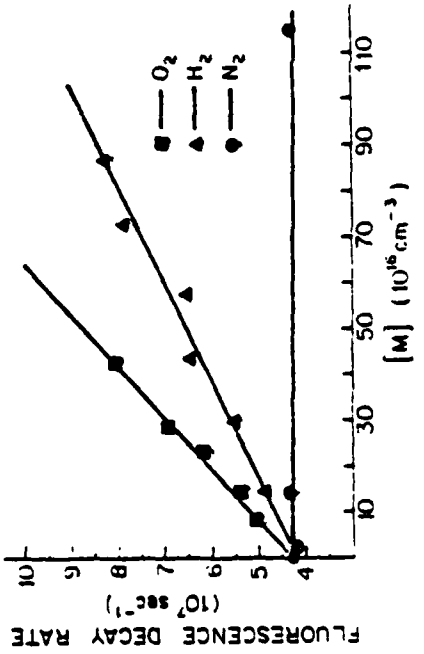

results shown in Table (II-2) were obtained by monitoring the total fluorescence from the (B) state. This may include small contributions from different vibrational levels within the (B) state. Using a 0.75 m monochromator (0.1 nm resolution), it was possible to observe at various wavelengths and measure such lifetimes where the transitions from specific vibrational states are more prominent. The measured lifetimes for v'=0,3, and 6 are 24±1, 22±1 and 23±1 ns respectively, indicating only a very slight variation, if any, in radiative lifetime with vibrational excitation. When monitoring the total fluorescence from the (B) state, an averaged lifetime of 22.7 ns was measured. It is common when measuring lifetimes to consider the effects of self trapping. Self trapping is directly a function of the photon collection geometry, parameters such as the number density (optical density) and the path length of the escaping radiation are critical in determining the extent of radiation imprisonment (self trapping). Since the measured results for the radiative lifetime agrees with the results of others,[2,12] the extent to which radiation is trapped is minimal.

TABLE (II-2). Rate coefficients for the quenching of HgBr($B^2\Sigma^+_{1/2}$).

quenching species	rate coefficient this work[a] (378 K)	($\times 10^{-11}$ cm^3 molecule sec^{-1}) other work	Ref.	Comments
$HgBr_2$	(23.0±6.0)	(17.0±3.0)	14	may react
CO	(3.4±0.6)			non-reactive
CO_2	(3.7±0.3)			non-reactive
O_2	(9.2±0.3)			may react
H_2	(4.8±0.6)			may react
Br_2	(31.0±4.0)	(29.0)	13	may react
		(55.0±3.0)	14	
Xe	(0.02±0.004)	(0.03)	13	non-reactive
		(0.37±0.03)	14	
N_2	≤ 0.015	(≤0.0063)	13	non-reactive
		(0.44±0.05)		

[a]The quoted uncertainties are statistical, and are two standard deviations.

Discussion

The rate coefficients obtained are in reasonable agreement with those from certain other experiments in those cases where comparison is possible (Table (II-2)). There are obvious differences between these measurements, as well as those of Mandl,[13] and the measurements of Eden et al.[14] These differences are particularly striking for quenching by Xe and N_2. When measuring an inefficient quenching process, sample purity becomes paramount. The trace impurities usually found in both Xe and N_2 gases are O_2, H_2, CO, CO_2 and H_2O.[15] Of the five impurities listed, the first four are known to be efficient quenchers of HgBr(B) (Table II-2)). So great care must be taken to purge all gas lines with ample high grade Xe and N_2 to insure that trace impurities are kept at a base minimum.

As reported in Table (II-2), quenching rate coefficients for the species $HgBr_2$, CO, CO_2, O_2, H_2, and Br_2 are larger, by orders of magnitude, than the quenching rate coefficients for species such as Xe and N_2. It seems unlikely that the efficient quenching of HgBr(B) produces ground state HgBr species. This would require greater than 2.85 eV of excitation to be taken up

by internal states of the quenching species and relative translation between HgBr and the quenching species. Usually electronic to vibrational (E-V) energy transfer rates are only efficient when the two states are in near energy resonance,[16,17] while electronic to translational (E-T) energy transfer rates are efficient when there are long range interactions between the colliding pair.[18] Other alternatives to the quenching of HgBr(B) which are more likely, are reactive collisions (HgBr+O_2 —> HgO+BrO) or collision induced dissociation (HgBr(B)+O_2 —> Hg+Br+O_2). It is possible to assess the contributions of these channels by laser induced fluorescence (LIF) of BrO (BrO(X-A) Te = 24,933 cm^{-1}) and Hg (Hg(6^1S_0) —> Hg(6^3P_1) E = 4.88 eV). CO and CO_2 are efficient quenchers even though chemical reaction can not occur, here it is believed that collisions with HgBr(B) result in a transition to a dissociative potential curve of HgBr (HgBr($A^2\Sigma$) is a repulsive surface which has 2-fold degeneracy[19] (see Fig. (I-2)). It is unclear at this time, why N_2 is far less efficient at inducing this transition. At first inclination, one would expect CO and N_2 to behave similarly since they are isoelectronic, but in fact the charge distribution in N_2 is symmetric while in CO it is

clearly not. This asymmetry in charge distribution for CO may be reflected by its ability to form localized bonds which can enhance the interaction with the electronically excited radical. In N_2 any bond formation will have to be symmetrically distributed over the molecule, and will lead to a weaker interaction. The stronger attractive interaction of HgBr(B) with CO can cause the potential energy surface, those which connect the initial and final states, to converge with that of lower electronic state.[20] There have been other reported cases in which N_2 and CO behave differently. In the quenching of the ^3P_J states of Cd where no accessible electronic states exist for either CO or N_2, CO was found to be a far more efficient quenching partner than N_2.[21]

References (Chapter VI)

[1]B.E. Wilcomb, R. Burnham, N. Djeu, Chem. Phys. Lett. 71, 239 (1980).

[2]R.W. Waynant, J.G. Eden, Appl. Phys. Lett. 11, 708 (1978).

[3]K. Wieland, Z. Elektrochem. 64, 761 (1960).

[4]N. Cheung, T.A. Cool, J. Quant. Spectrosc. Radiat. Transfer 21, 397 (1979).

[5]R. Weast, ed., Handbook of Chemistry and Physics (Chemical Rubber Co., Cleveland, 1973).

[6]R.E. Weston, Jr., H.A. Schwarz, Chemical Kinetics (Prentice-Hall Inc., New Jersey, 1972).

[7]M. Ogawa, J. Chem. Phys. 54, 2550 (1971).

[8]G. Herzberg, Molecular Spectra and Molecular Structure: I. Spectra of Diatomic Molecules (Van Nostrand Reinhold, New York, 1950).

[9]C. Rozlo, A. Mandl, J. Appl. Phys. 51, 2969 (1980).

[10]T.A. Cool, J.A. McGarvey, Jr., A.C. Erlandson, Chem. Phys. Lett. 58, 108 (1978).

[11]J.G. Calvert, J.N. Pitts, Jr., Photochemistry (John Wiley & Sons, Inc., New York, 1967).

[12]N. Djeu, C. Massa, Chem. Phys. Lett. 46, 172 (1977).

[13]A. Mandl, J.H. Parks, C. Rozlo, J. Chem. Phys. 72, 504 (1980).

[14]J.G. Eden, R.W. Waynant, Appl. Phys. Lett. 14, 324 (1979).

[15]Physical and Chemical Gas Data Chart, Liquid Carbonic Corporation, 1976.

[16]R.J. Donovan, Laser-Induced Processes in Molecules, K.L. Kompa, S.D. Smith eds., (Springer-Verlag, New York, pg. 324, 1979).

[17]A.B. Callear, Gas Kinetics and Energy Transfer Specialist Periodical Reports, Vol. 3 (The Chemical Society, Billing & Sons Ltd., London, 1978).

[18]W.H. Breckenridge, H. Umemoto, Advances in Chemical Physics The Dynamics of the Excited State, K. Lawley, ed., (in press).

[19]W.R. Wadt, Appl. Phys. Lett. 34, 658 (1979).

[20]A.B. Callear, J.D. Lambert, Comprehensive Chemical Kinetics, Vol. 3 (Elsevier, Amsterdam, 1969).

[21]W.H. Breckenridge, A.M. Renlund, J. Phys. Chem. 83, 1474 (1978).

CHAPTER III

VIBRATIONAL DEACTIVATION OF HgBr($X^2\Sigma^+_{1/2}$,v^*)

Introduction

There are collisional processes associated with the ground state HgBr species, further labelled as HgBr(X), which are pertinent to the efficiency of HgBr(B→X) lasers. One such process is the collisional deactivation of the ground laser level. The HgBr laser operates from the low v' levels of the (B) state to high v'' (v''=18-24) levels of the (X) electronic state.[1] To prevent "bottlenecking" and self termination of the laser, it is imperative that their be efficient removal of the ground state population. In examining the collisional quenching of these high vibrational states, one can also obtain information on the transfer of energy from vibrational restoring forces to translational energies. Vibrationally excited HgBr(X,v'') molecules have a high probability of giving up one or more vibrational quanta of energy if involved

in a collision ($h\nu$ at $v''=22$ is 140 cm^{-1} while kT at 300 K is 200 cm^{-1}).[2]

There are various schemes with which ground state radicals can be monitored. Four general processes are mentioned. HgBr(X) radicals can be monitored through 1) reactive processes (where one or more reaction products are observed), 2) ionization processes (electron impact or other charge transfer processes which leave ionized or excited species that can be monitored), 3) energy transfer processes (long range interactions or shockwave excitation which excite the ground state radical), and 4) laser induced fluorescence (LIF: the excitation and subsequent remission of species via optical excitation, i.e. laser). Of the four processes mentioned, the probing of ground state radicals via LIF has particular appeal, because the technique can provide information on quantum systems with minimum perturbation of the ensemble.[3] It is limited by the accessibility of the desired radiation wavelength, and the magnitude of the transition coupling matrix element. The simple equations which relate the LIF emission intensity to the various quantum parameters are given below. If given that there are N_m species (number/cm^3) in an initial lower state (m) and that I_0^{nm} is the intensity

(erg/cm^2-sec) of the incident radiation with frequency ν_{nm}, then the intensity of absorption I_{ab}^{nm} can be simply written as

$$I_{ab}^{nm} = I_0^{nm} N_m B_{nm} h\nu_{nm} \Delta X \qquad (1)$$

where B_{nm} is the Einstein transition probability for absorption and ΔX is the thickness of the absorbing layer (the incident radiation here is assumed to have a constant intensity over the whole absorption line width). Subsequent to this absorption, a population $I_{ab}^{nm}/(h\nu_{nm})$ is formed in the excited state (n). Neglecting collisional effects, species in state (n) can emit radiation at a rate given by

$$I_{em}^{mn} = N_n h\nu_{mn} A_{mn} \qquad (2)$$

where N_n is again the population in state (n), ν_{mn} the emission frequency, and A_{mn} the transition probability (Einstein A coefficient. A_{mn} is proportional to $(\langle s/R/n \rangle)^2$ where R is the matrix element for the transition). If one combines Equations (1) and (2), the emission intensity I_{em}^{mn} is related to the initial population N_n by the equation

$$I_{em}^{mn} = (I_0^{nm} B_{nm} A_{mn} h\nu_{mn} \Delta X) N_n \qquad (3)$$

In order to measure N_n absolutely, it is necessary to know all the corresponding terms in Equation (3), but for a constant I_0^{nm} and ΔX, the parenthetical product is invariant. This provides for a method with which to measure relative population changes in state (n). LIF enhances the technique by insuring a large incident photon flux and a high degree of monochromacity.

In this chapter results are presented for the collisional deactivation of groups of vibrational levels in HgBr(X) via LIF. In HgBr(X) species, it is not possible to optically monitor individual transitions, but it is possible to monitor combinations of v'' levels simultaneously. From computer calculations, the relative absorption of the strongest vibrational transitions within each group are determined. Two sets of experiments are discussed. The first experiment, gives results on the time evolution of three different groups of vibrational level densities which are quenched by He. The results show that vibrational quenching is efficient down to the lowest v'' levels that were monitored. In the second experiment, results are presented wherein the rate coefficients are measured for the net removal of vibrational densities in the lower HgBr(B→X) laser levels ($v'' \sim 22$) by various species.

The rate coefficients are large indicating that deactivation of the lower laser levels proceeds efficiently. These measured rate coefficients, for the collisional quenching, are recast to show some correlation with the polarizibility of the quenching partner, and furthermore, the Absorbing-Sphere model with van der Waals interaction is presented as a possible scheme for describing the quenching mechanism.

Experimental

The experimental arrangement is shown schematically in Fig. (III-1). Vibrationally excited HgBr(X,v'') molecules are produced via ArF laser photolysis of $HgBr_2$ vapor at 193 nm:[1]

$$HgBr_2 + h\nu(193\ nm) \longrightarrow HgBr(B) + Br(^2P_{1/2,3/2}) \qquad (3)$$

$$HgBr(B) \longrightarrow HgBr(X,v'') + h\nu \qquad (4)$$

Different groups of v'' levels are monitored via LIF using a pulsed dye laser. The time evolution of the various groups of v'' levels can be monitored by varying the delay between the photolysis and dye lasers and recording the change in the peak LIF signal.

FIG. (III-1). Schematic drawing of the experimental arrangement. A typical datum from the transient digitizer/signal averager showing LIF following ArF laser photolysis of $HgBr_2$ is indicated in the upper left hand corner. Time evolution is obtained by varying the delay between the ArF and dye lasers. Each datum is an average of 256 traces. The gated PMT discriminates against the "t=0" emission and makes the "t=0" and LIF signals comparable in magnitude.

The sample chamber, detector and recording electronics are inside a large screen room (Faraday Cage) which provides adequate isolation from the electrically noisy laser sources. The output from the ArF laser Lumonics, 193 nm, 100 mJ, 20 ns fwhm) is sent into the screen room and enters the chamber unfocussed through Suprasil quartz windows. After a preset delay, a N_2 laser pumped dye laser (NRG, 0.2 mJ, 0.01 nm resolution) is directed into the chamber and crosses the ArF laser at right angles in the center of the chamber. LIF is observed at right angles to both lasers using either a telescope/gated PMT (EMI, 9659 QB, 165-900 nm, 10 ns rise time and 1 μs gate response time) arrangement or a telescope/monochromator/PMT (RCA, 8575, 260-880 nm, 1 ns rise time) set up. The monochromator (Jarrel-Ash, 2 nm resolution) and gated PMT are used to discriminate against the B-->X emission from reaction (4). Signals from the PMT are digitized and averaged (Biomation, Tracor Northern, 10 ns gate or the Nicolet, 100 ns gate) until adequate signal to noise (S/N) is obtained. A typical signal averaged datum is shown in the corner of Fig. (III-1).

LIF experiments are usually plagued by copious amounts of scattered laser light. To alleviate this

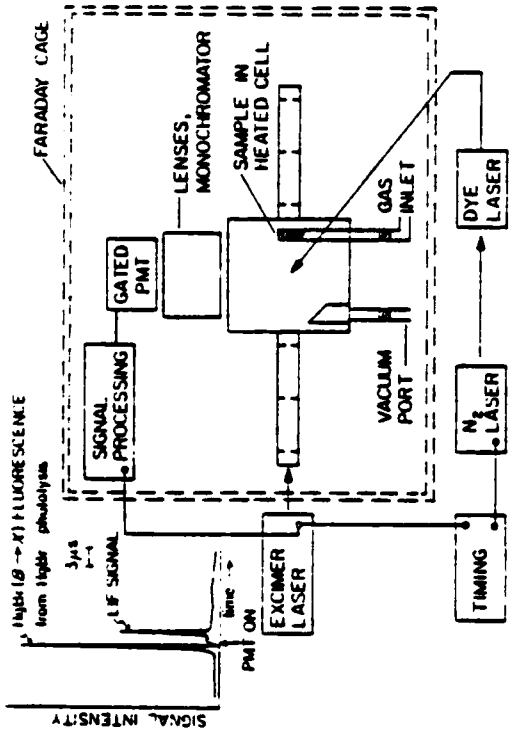

problem, it becomes of paramount importance to design and build a fluorescence chamber where scattered light can be efficiently rejected (Fig. (III-1)).[5]

The square "pillbox" in the center has a volume of 20x20x20 cm^3 and is made of black anodized aluminum. Aluminum can be easily machined and has reasonable corrosion rates, when in contact with mercury compounds (Table (III-1) gives some corrosion data). On top of the chamber there is a carefully machined flange which mates with a telescope, the monochromator and gated PMT apparatus. In the telescope section there are also three trays which allow quick insertion of filters, lenses, etc. in the observation path. The four arms, each 40 cm long, are structurally bolted to the chamber. There are also O ring seals which allow evacuation of the arms. In each arm there are several baffles placed in sequence, each baffle in the sequence has a slightly smaller aperture size. Laser light entering the arm gets gently tapered by the sequence of baffles. The chamber, telescope and arms efficiently reject all forms of scattered light, allowing the convenience of doing experiments with the room lights on. Inside the chamber and in one corner is a glass cuvette. It is filled with glass beads (2 mm Dia, to enhance gas mixing) and the

TABLE (III-1). Corrosion Data for Metals and Non Metals with Br_2 and $HgBr_2$.[a]

Metals/ NonMetals	Br_2 (penetration/year)	$HgBr_2$ (penetration/year)
Aluminum	<20 mills (60-220°F)	>50 mills (60-100°F)
Tantalum	<2 mills (60-300°F)	<2 mills (60-200°F)
Brass		>50 mills (60-100°F)
Bronz		>50 mills (60-100°F)
Copper		>50 mills (60-100°F)
Stainless (Steel,316)		<20 mills (60-140°F)
Borosilicate (non metal)	resistant (60-200°F)	resistant (60-100°F)

[a]Reference (6).

$HgBr_2$ sample (white powder). The cuvette is also wrapped with nichrome wire which allows the sample to be heated to temperatures exceeding 373 K (100 mTorr of $HgBr_2$). Quenching gases are brought in from the bottom of the cuvette and mix with $HgBr_2$ vapor. The saturated gas exits through several fine nozzles located on top of the cuvette. The nozzles insure that a slow flow of the mixture will pass directly through the observation region. The chamber and arms are evacuated using a 500 l/min rough pump with a liquid N_2 cold trap filled with copper turnings. The cold trap serves to both protect the pump, by trapping out corrosive gases and also to inhibit oil vapor from the pump in reaching the fluorescence chamber. Total pressure in the chamber is measured with a capacitance manometer (MKS 222 BS-P-10) and temperture is measured with a thermocouple located at the exit port of the cuvette. The chamber is continuously pumped in order to minimize $HgBr_2$ condensation on the walls and the long baffled arms further prevent condensation on the windows. The present experiments were done either 330 K or 335 K,[7] providing a HgBr density of approximately 10^{12} and 10^{13} cm^{-3}.[8] At this density of parent species, quenching of HgBr(X,v") by undissociated parent molecules or photofragments contributes only a very small amount to the *observed quenching*.

$HgBr_2$ is Baker Analyzed Reagent Grade and all other gases are Airco research grade (99.995% min).

Results

HgBr(X) molecules in high vibrational levels are produced via reactions (3) and (4). These species are subsequently deexcited by molecular collisions and this relaxation can be monitored via LIF from different v" levels. Since the dye laser may simultaneously excite molecues from several v", the measurements provide only the time evolution of groups of v" levels. This can be seen in Fig. (III-2), where shown are the vibrational levels which are simultaneously monitored at the probe frequencies used in the experiment. (see Appendix A for a summary and discussion on the calculations in generating *Figs. (III-2(a-d))*. This overlap of various vibrational transitions is unfortunate, but inevitable given the high state and spectral densities of HgBr. Three probe frequencies were used, they correspond to high, intermediate and low v". Figure (III-3) shows data wherein the time evolutions of the three groups of

FIG. (III-2). Computer calculations of the absorptions of various bands for LIF at (a) 20,362 cm^{-1}, (b) 24,659 cm^{-1}, and (c)-(d) 19,924 cm^{-1}. Absorptions follow a Hund's case (a) coupling scheme for a $^2\Sigma^+ - {}^2\Sigma^+$ transition in $Hg^{79}Br$. Line strengths are from Kovacs[9] and the curves were generated by summing 120 rotational levels at a temperature of 300 K. The absorptions of the other abundant isotope, $Hg^{81}Br$, are shifted 2 cm^{-1} to the blue. In (a)-(c), a flat distribution of v" populations is used to indicate the largest Franck-Condon factors near the probe frequency. In (d), nascent v" populations produced via reactions (3) and (4) are used. Here, nascent v' populations are mapped onto the v" levels using known Franck-Condon factors. Note that *each group* of v" has its own set of arbitrary units.

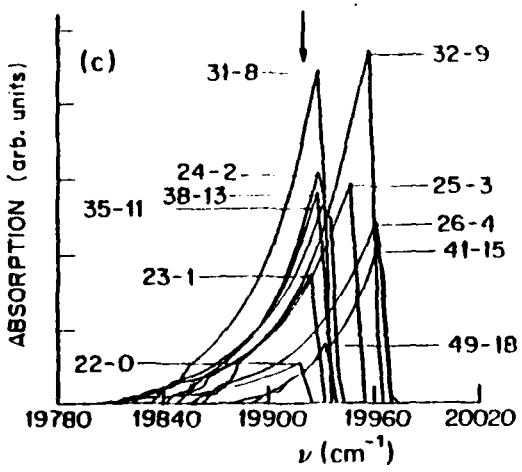
(c)
31-8
32-9
24-2
25-3
35-11
38-13
26-4
41-15
23-1
49-18
22-0
ABSORPTION (arb. units)
19780
19840
19900
19960
20020
ν (cm⁻¹)

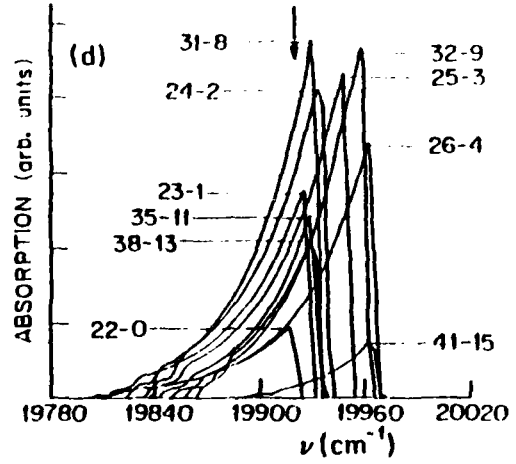
(d)
31-8
32-9
24-2
25-3
26-4
23-1
35-11
38-13
22-0
41-15
ABSORPTION (arb. units)
19780
19840
19900
19960
20020
ν (cm⁻¹)

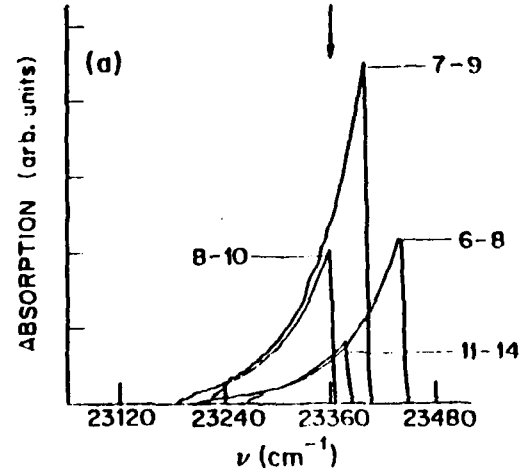
(a)
7-9
8-10
6-8
11-14
ABSORPTION (arb. units)
23120
23240
23360
23480
ν (cm⁻¹)

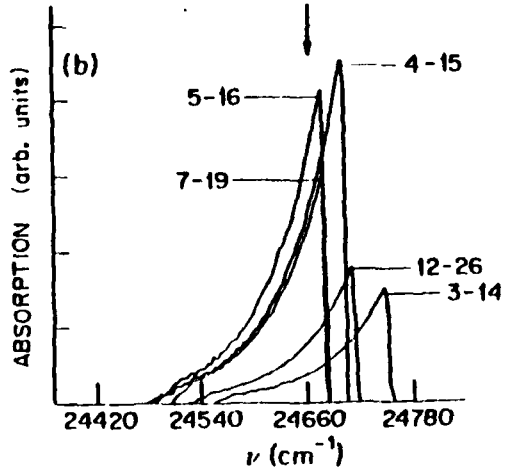
(b)
4-15
5-16
7-19
12-26
3-14
ABSORPTION (arb. units)
24420
24540
24660
24780
ν (cm⁻¹)

v° levels are monitored. Vibrational deexcitation is due to collisions with He in these experiments. The concentration of [He] is much greater than [$HgBr_2$], so deactivation by parent species is expected to have a negligible effect. The temporal shapes shown in Fig.(III-3) are complex, especially for Figs. (III-3b and 3c). Although state specific rate coefficients cannot be extracted from such data, there are several relevant conclusions which can be drawn and these are summarized here.

(i) For ν =23,362 cm^{-1} (the *intermediate group*), one primarily monitors v°=7 and 8, with smaller contributions from v°=6 and 11 (see Fig. (III-2a)). These levels are scantly populated at t=0, but develop larger populations as the higher v° levels are efficiently deexcited. The rise portion of Fig. (III-3b) depicts the filling of these levels from upper vibrational states. The rise time of the signal varies with [He], and the slope of τ_{rise} vs. [He] is linear and equal to $2.5 \times 10^7 s^{-1} Torr^{-1}$ (see Fig. (III-4)). This indicates that molecules are efficiently transported to intermediate vibrational levels, but it is not possible to infer state specific rate coefficients from such data. The rather flat region (t > 5 us) is interpreted

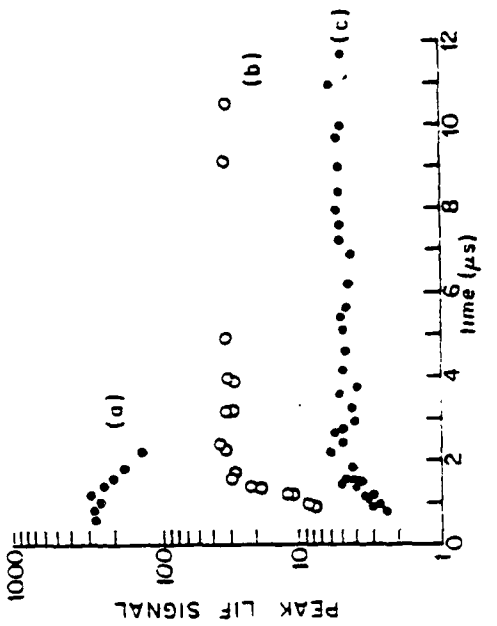

FIG. (III-3). Time evolution of the peak LIF signal, monitored by varying the delay between photolysis and dye lasers; t=0 is coincident with the termination of the ArF laser output. The dye laser probe frequencies are (a) 19,926 cm^{-1}, (b) 23,362 cm^{-1}, (c) 24,659 cm^{-1}. Each point in (a), and the rise portions of (b) and (c) represents an average over 2048 laser firings, while 512 firings were adequate for points in the flat portions of (b) and (c). The data shown in (a), (b) and (c) are offset from one another for convenience; vertical scales (in arb. units) are valid <u>within</u> each of these sets of data but not <u>between</u> different sets of data.

FIG. (III-4). A least squares fit of the "initial rise" portion of the curves in Fig.(III-3) vs. He pressure. The rise portion describes filling of vibrational levels which are originally scantly populated.

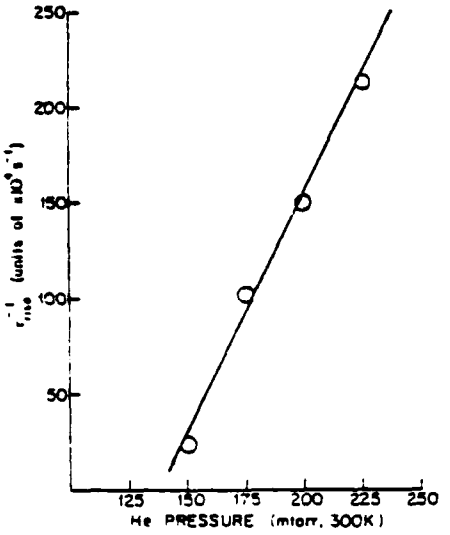

as a quasi steady-state situation in which molecules are entering and leaving intermediate v'' levels with comparable rates. Although not shown in Fig. (III-3b), the LIF signal falls rather quickly following the "flat" portions shown in Figs. (III-3b,3c) (net removal rate coefficient $\sim 4\times10^5 s^{-1}Torr^{-1}$). This is in further agreement with the flat portion depicting a quasi-steady-state situation.

(ii) For ν =24,659 cm^{-1} one primarily monitors v''=4,5 and 7, with smaller contributions from v''=3 and 12 (see Fig. (III-3c). Qualitatively the behavior is the same as with =23,362 cm^{-1}, indicating that molecules are rapidly transported to these low vibrational levels by collisions with He.

(iii) For ν = 19,924 cm^{-1}, (high v''), vibrational levels with v''>22 are monitored. Analysis of these states requires more careful scrutiny because vibrational levels near v''=22 also define the lower HgBr(B-->X) laser level. In Fig. (III-2d) the relative absorptions of various bands for LIF at 19,924 cm^{-1} have been calculated using nascent v'' levels produced via reactions (3) and (4). Thus ground state distribution is derived by mapping the nascent v' levels onto v'' levels using known Franck-Condon factors [10] (see

Appendix B for detailed discussion). As one can see from Fig. (III-2d) that all absorptions are from molecules v''>22. Molecules with v''<22 have absorption peaks far removed from the dye laser frequency, making v''=22 the lowest level monitored in this <u>group</u>. v''=22 also happens to be the ground state for one of the strongest transitions in the HgBr(B-->X) laser. Therefore, after a number of collisions, absorption from v''>22 will decrease relative to absorption near v''=22. The LIF time evolution (see Fig. (III-3a)) exhibits this by non-exponential character at short times, followed by a long, rather exponential tail. This is indicative of the net removal of molecules through v''=22. Though state specific rate coefficients are not possible, rate coefficients for the net collisional removal of these levels can be measured. In a subsequent experiment these rate coefficients were measured for various collisional partners.

In the following experiments (all at ν=19.924 cm^{-1}), all the quenching species [M_i], which were chosen have small absorption cross sections at 193 nm,[2,11] insuring that photoproducts from M_i do not play an important role in the experiment. In addition, since the physical quenching of the HgBr(B) state can proceed through

several distinct pathways, it is important that the collisional relaxation of HgBr(B) be minimized. By using low concentrations of M_i, one could be reasonably sure that the probability of a collision and possible deactivation is small. The removal of HgBr(X,v'') by collisions is complex and can generally be represented by(for a given M).

$$d/dt\,[HgBr(X,v'')] = \sum_{i=1}^{I} \{k_M^{v''+i,v''}[HgBr(X,v''+i)] - k_M^{v'',v''+i}[HgBr(X,v'')]\}[M] \quad (5)$$

$$\sum_{j=1}^{J} \{k_M^{v'',v''-j}[HgBr(X,v'')] - k_M^{v''-j,v''}[HgBr(X,v''-j)]\}[M]$$

where v'' is a particular vibrational level of HgBr(X), $k^{v''+i,v''}$ is the rate coefficient for collsional energy transfer from the state $v''+i$ to the state v'', and I and J represent the maximum number of participating states above and below v'' respectively. It was assumed that all quenching is via collisions with M and that the rate of diffusion out of the laser beams is small compared to the rate of collisional quenching, which is true under

the conditins of the experiment. Equation (5) shows both forward and reverse processes since the vibrational quanta are very small (140 cm^{-1} at v°=22 , with kT~ 245 cm^{-1}).

With both source and loss terms in Equation (5), it becomes impossible to determine state specific rate coefficients by measuring [HgBr(X,v°)](t). But fortunately, by doing LIF at ν = 19,924 cm^{-1} one really probes v°>22, so it is then possible to measure the net removal of HgBr(X,v°) through v°=22. The experimental signals do show exponential decay (see Fig. (III-5)) supporting those calculations which show v°=22 to be the lowest vibrational level probed in the ensemble (see Fig. (III-2)). The removal of HgBr(X,v°) by M species can be fit by the equation.

$$k'_M = k_M[M] \qquad (6)$$

where k_M bears no simple relationship to the k in Eq. (5). Nevertheless, k_M indicates qualitatively the rate coefficients of Eq. (4) and is in fact the more relevant parameter as far as HgBr laser operation is concerned.

Typical data from which k_M are derived are shown in Fig. (III-6) and the results are summarized in Table (III-2). The rate coefficients are very large for all the quenching species used. These very large rate

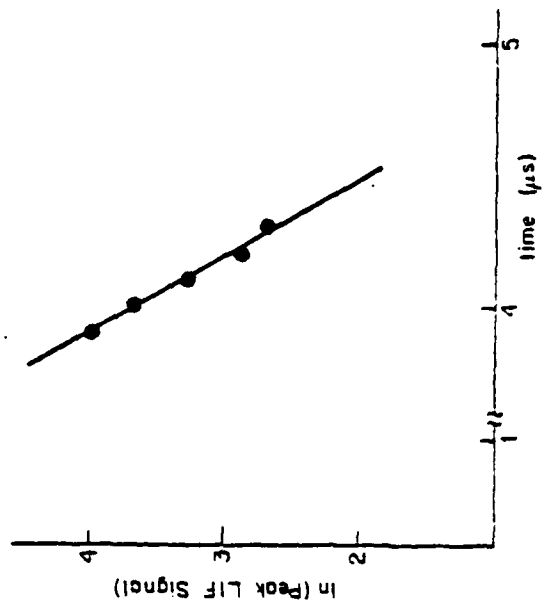

FIG. (III-5). Time evolution of the peak LIF signal as monitored by varying the delay between photolysis and dye lasers. Each point represents an average of 512 traces, with the origin of the time scale coincident with the termination of the ArF laser pulse. The data shown, were taken with 3 mTorr $HgBr_2$ and 1.2 Torr N_2.

FIG. (III-6). Typical data from which $k^{v^{\circ}=22}$ for Ar are derived. The curvature at low pressure shows the effect of Ar in limiting diffusion of HgBr from the observation region. Allowing for random and systematic errors, the uncertainty in the slope is $\leq$ 10%.

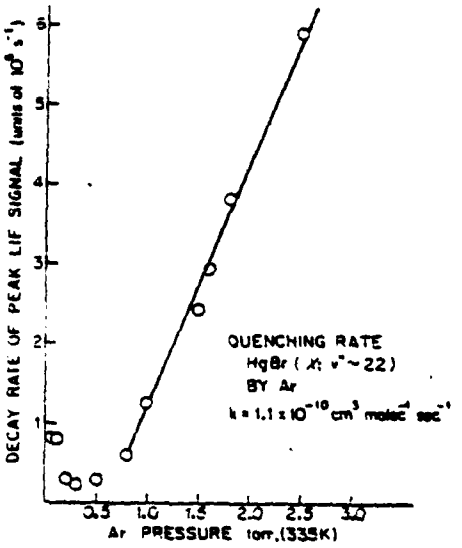

coefficients for the net removal through v"=22 indicate that the lower HgBr(B—>X) laser level is very efficiently deactivated in the laser environment and there should be no self-termination of the laser output due to "metastable" vibrationally excited molecules in the ground electronic state. Furthermore, in the laser environment (several atm.), vibrational relaxation of the entire $X^2\Sigma^+_{1/2}$ manifold will be complete in a few ns. Thus, in any practical HgBr laser device, energy can be extracted from the laser even when tuning to frequencies other than those with the highest gain.

Discussion

It is often pleasing, at least from a personal point of view, to rationalize one's measurements in light of existing theories. This is an unusually arduous task in the present situation and only certain features will be mentioned which seem reasonable and worth pointing out. First, the very small vibrational quanta are consistent with efficient vibration <—> translation exchange, since HgBr restoring forces are comparable to the HgBr-R forces experienced during collisions ($F \sim 10^{-4}$ dyne, see Appendix C). Second, HgBr

TABLE (III-2). Rate coefficients and probabilities for the net removal of HgBr(X, v"=22).

quenching species	rate coefficient[a] (335K) in units of 10^{-11} cm^3 $molec^{-1}s^{-1}$	probability[a,b]	polarizability[c] units of 10^{-24} cm^3
He	4.4	0.084	0.204
Ne	6.9	0.264	0.400
Ar	11	0.498	1.64
Kr	11	0.675	2.48
Xe	14	0.874	4.04
H_2	11	0.134	0.79
N_2	18	0.642	1.76
O_2	21	0.665	1.60

[a] We estimate an experimental uncertainty of ±10%, including random and possible systematic errors.

[b] The probability for the net removal of HgBr(X,v"=22) is defined by $P = \frac{k}{(\bar{v}\sigma_0^2)} = k/((8RT/\pi\mu)^{1/2}(r_R+r_{HgBr})^2)$ where k is the rate coefficient, μ is the collision reduced mass, and r_R and r_{HgBr} are the gas kinetic radii.[12]

[c] Polarizabilities are taken from Ref. (13).

has a large dipole moment (2.6D)[14] and the trends manifest in Table (III-2) show an interesting correlation between polarizability and energy transfer probability (see Fig.(III-7)). The observed trend gives confidence to try testing two appropriate quenching models for the deactivation of HgBr(X,v") species. Both models use the attractive van der Waals dispersion force ($-C_6/r^6$) as the interaction potential. For the simple case of two interacting particles, the quenching mechanism in the first model (Orbiting model)[4,15] assumes that a fraction of χ of those incoming trajectories with initial kinetic energy E which surmount the centrifugal barrier lead to quenching. The effective potential and the cross section are given by the equations.

$$V_{eff} = -C_6/r^6 + Eb^2/r^2 \qquad (7)$$

$$\sigma_Q = \chi b^2 = \chi\pi(3/2)(2C_6/E)^{1/3} \qquad (8)$$

The position of the barrier (at r_0) as well as the critical impact parameter b, for energy E can be determined by the simultaneous relations $(V_{eff})_0 = E$ and $(dV_{eff}/dr)_0 = 0$.

Closely related to the Orbiting model is the Absorbing-Sphere model,[4,16-18] which assumes that all collisions reaching a critical distance r_c lead to

FIG. (III-7). The probability of net removal of HgBr(X,v"-22) vs. polarizability of the quenching molecule. The probabilities show an almost monotonic increase with increasing polarizability.

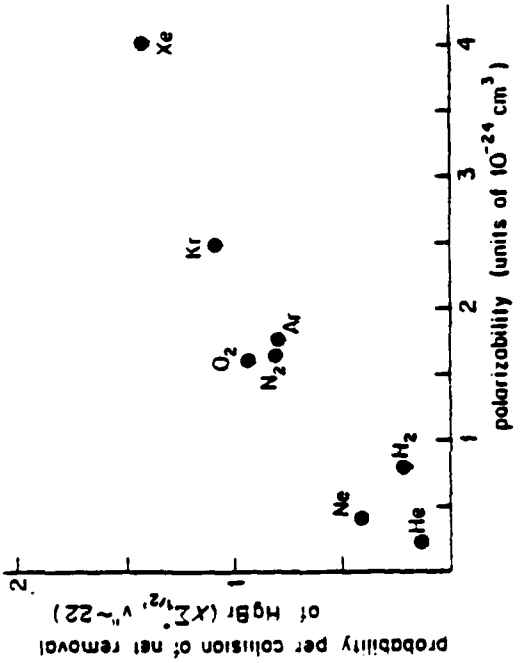

quenching. Using Eq. (7), the cross section for the Absorbing-Sphere model is given by:

$$\sigma_Q = \pi b^2 = \pi r_c^2(1+C_6/(Er_c^6)) \qquad (9)$$

By calculating the C_6 interaction coefficient for the various quenching partners of HgBr(X,v"), one can test to see which model more closely resembles the quenching of HgBr(X,v"). A plot of $\ln(\sigma_Q)$ vs. $\ln(C_6)$ predicts a slope of 1/3 for the orbiting mechanism, and unit slope for the Absorbing-Sphere model.

The experimental results of Table (III-2) were plotted against calculated C_6 coefficients. The σ_Q were calculated using the relation $\sigma_Q = k_M/\langle v_M \rangle$, where k_M is the measured quenching rate coefficient and $\langle v_M \rangle$ is the average collision velocity. The C_6 coefficients were calculated using the London formula.[19,20] The London formula gives C_6 values which are found to be 15-20% smaller than the more reliable Slater-Kirkwood formula.[19] The Slater-Kirkwood formula was not used because it is more cumbersome.[21] This discrepancy between formulae was removed by increasing all calculated C_6 values by 20%. Listed below are the equations used and Table (III-3) lists the necessary parameters and results. For two interacting species (a) and (b), the C_6 is given by,

TABLE (III-3). The C_6 coefficients for the interaction of HgBr(X,v") + M.

Quenching species	Polarizability[a] (10^{-24}cm^3)	Ionization[b] Potential (10^{-11}ergs)	C_{aa} (x10^{58} ergs-cm^6)	C_6 (x10^{-57} ergs-cm^6)
HgBr	65.0[c]	1.94[d]	737.0	
He	0.204	3.92	0.0146	0.308
Ne	0.40	3.45	0.0496	0.580
Ar	1.64	2.52	0.61	2.10
Kr	2.48	2.24	1.23	3.00
Xe	4.04	1.94	2.84	4.88
H_2	0.79	2.47	0.138	1.00
N_2	1.76	2.49	0.69	2.23
O_2	1.60	1.93	0.44	1.80

[a]Reference (13)
[b]Reference (8)
[c]Reference (22)
[d]Reference (23)

$$C_6 = C_{ab} = 2C_{aa}C_{bb}/[(\alpha_b/\alpha_a)C_{aa} + (\alpha_a/\alpha_b)C_{bb}] \quad (10)$$

and using the London formula,

$$C_{aa} = 3/4(\alpha_a^2)(I.P) \quad (11)$$

where α_a, α_b are the respective polarizabilities for species (a) and (b), (I.P) is the species ionization potential and C_{aa} or C_{bb} are the C's for like interactions.

In figure (III-8), a plot of $\ln(\sigma_Q)$ vs. $\ln(C_6)$ shows the data to be more in alignment with the line of slope 1. Although various approximations were used in testing of these two quenching models, the observed nearly linear dependence of σ_Q on C_6 could imply that the Absorbing-Sphere model is more appropriate for the quenching of vibrationally excited HgBr(X) species by the various reagents tested. This result gives further credance to the claim that HgBr restoring forces are comparable to HgBr+M forces. In such collisions, one expects <u>all</u> incoming trajectories and not just a partial <u>fraction</u>, which pass the critical distance, to lead to quenching.

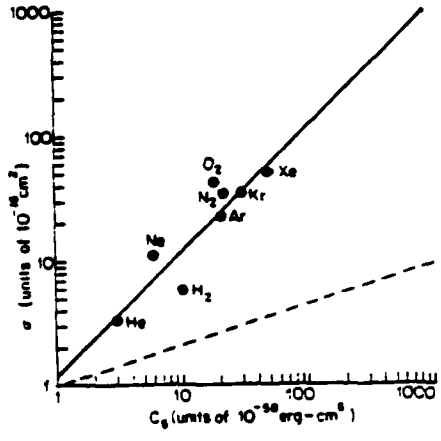

FIG. (III-8). A plot of the cross section σ vs. the C_6 interaction coefficient. σ is defined by $k/\langle v\rangle$ where k is the measured quenching rate coefficient and $\langle v\rangle$ is the average collision velocity defined by $\langle v\rangle = (8kT/\pi u)^{1/2}$ where u is the collision reduced mass and T= 335 K. The solid line has unit slope while the dashed is drawn with slope 1/3.

Appendix A: <u>Outline for simulation of relative absorption by LIF of various bands in HgBr($X^2\Sigma^+_{1/2}$)</u>.

Rather than just display the computer program used in the simulation studies, it is perhaps better to outline the crucial steps, listing the important equations and discussing the limitations and results of the computer program. In this appendix an outline is presented for simulating optical transitions from v" states of ($X^2\Sigma^+_{1/2}$) to v' states of ($B^2\Sigma^+_{1/2}$) in $Hg^{79}Br$. It is expected that the wavelengths for all similar transitions in the other abundant isotope $Hg^{81}Br$ will be shifted toward the blue (higher energies) by 2 cm^{-1}. Any realistic analysis of optical absorption in HgBr(X) must include isotopic effects. The following analysis is prepared only to show the general absorption characteristics of the radical HgBr. The influence of molecular rotation on electronic motion are considered by using the coupling scheme of Hund's case (b).[2] In this case the spin S vector is either weakly or not coupled to the internuclear axis. The total angular momentum apart from spin is designated by the letter R. Inclusion of the spin S vector causes a 2S+1 splitting

of each K state (J=K+S). For a $^2\Sigma \longrightarrow {}^2\Sigma$ transition, there appears two R (J—>J+1) branches and two P (J—>J-1) branches. Using known spectroscopic constants, one can write the rotational term values for the Hund's case (b) coupled molecule. The two series (J-1/2,J+1/2) are given by.

$$F_1(K)=F_{(J+1/2)} = \nu_0+B_\nu K(K+1)-D_\nu K^2(K+1)^2-1/2\gamma(K+1) \quad (A1)$$

$$F_2(K)=F_{(J-1/2)} = \nu_0+B_\nu K(K+1)-D_\nu K^2(K+1)^2+1/2\gamma K \quad (A2)$$

where B_ν, D_ν and γ are the spectroscopic constants and ν_0 is the band origin. Using F_1, F_2 the following equations display the P and R type transitions between various energy states.

$$P_1 = \nu_0 + F_1'(K-1) - F_1''(K) \quad (A3)$$

$$R_1 = \nu_0 + F_1'(K+1) - F_1''(K) \quad (A4)$$

$$P_2 = \nu_0 + F_2'(K-1) - F_2''(K) \quad (A5)$$

$$R_2 = \nu_0 + F_2'(K+1) - F_2''(K) \quad (A6)$$

In general the intensity for absorption via dipole transition between two electronic states is given by:

$$I(\nu) = \frac{CN_{\nu''}(R_e^{\nu',\nu''})^2|\langle\nu'|\nu''\rangle|^2 S_{J',J''}\{e^{-F(J'')/(kT)}\}}{Q_r Q_\nu} \quad (A7)$$

where $N_{\nu''}$ is the population in the ground vibrational state ν'', $R_e^{\nu',\nu''}$ are derived from known $\bar{r}$ centroids,[24]

assuming a continuum of J states (the rotational constant for B_2Br is B - 0.04 cm^{-1}),[10]

$$Q_r = kT/B \quad (A12)$$

The spectroscopic constants $B_{\nu''}$ and $B_{\nu'}$ were also inputs into the simulation, while the second order rotational constants $D_{\nu''}$ and $D_{\nu'}$ are calculated using the equations.

$$D_\nu = D_e + B_e(\nu+1/2) \quad (A13)$$

$$D_e = 4B_e^3/\omega_e^2 \quad (A14)$$

where B_e and ω_e are known spectroscopic constants. Because the D terms are very small, the program did not include the ν dependence of $D_\nu(D_\nu - D_e)$. Using Equation (A14) the parameters $D_{\nu'}$ and $D_{\nu''}$ are 1.8×10^{-9} and 2.44×10^{-9} respectively. The splitting constant γ in Equations (A1), (A2) is very small especially compared to the B_ν term. In the program γ was assumed to be zero. Although this makes $F_1(K)=F_2(K)$, the "lack" of splitting does not necessarily mean that rotational terms from $F_1(K)$ and $F_2(K)$ cannot overlap. The splitting does linearly increase with K ($\gamma(K+1/2)$), but this effect is assumed to be negligible over the number of K levels considered.

A computer program was developed in BASIC which calculated I(ν) for a number of vibrational bands

$\langle\nu'|\nu''\rangle^2$ are the Franck-Condon[10] factors, and $S_{J',J''}$ is the line strength. The exponent term gives the relative number of molecules in the different rotational states. Q_r and Q_ν are the state vibrational, rotational sum (partition function), and C is a constant. In this simulation the vibrational population $N_{\nu''}$ is always an input, therefore Q_ν is a state sum. For instance in Figs. (III-2(a-c)) all $N_{\nu''}$ are initially assumed to be equal, indicating at a glance those transitions which are most probable because of large Franck-Condon factors. The variation of $R_e^{\nu',\nu''}$ with ν'' is expected to be small and in each simulation it was assumed to be constant for the ensemble of ν'' considered. Figs. (III-2(a-d)) show that the vibrational levels, which have strong absorption cross sections at the probed laser frequency are near each other. All Franck-Condon factors are inputs into the simulation and the line strengths, $S_{J',J''}$, for $^2\Sigma \longrightarrow {}^2\Sigma$ transition are taken from Kovacs.[9] They are listed below.

$$R_1 = (K+2)(K+1)/(K+3/2) \quad (A8)$$

$$R_2 = (K)(K+1)/(K+1/2) \quad (A9)$$

$$P_1 = (K+1)(K)/(K+1/2) \quad (A10)$$

$$P_2 = (K-1)(K)/(K-1/2) \quad (A11)$$

The rotational partition function Q_r is calculated

situated near the laser probe frequency. Each transition band was separately calculated using a given vibrational population, and a rotational temperature. The calculations included summing over 120 rotational levels. In essence, the computer program generates a linear vector matrix where each element of the matrix is the net absorption I(ν) for a particular transition line of a rotation-vibration band. The vector matrix includes all four branches (R_1,R_2,P_1,P_2) of the particular absorption band. Because of the large number of transition lines, the calculated vector matrix contains an enormous number of elements, making it quite impractical for plotting on any sensible scale. It was necessary to establish a mathematical slit function, whereby for a given slit width, this function would scan over the vector matrix reducing the number of elements by averaging over the slit width. Within the slit width, the integration is a weighted average with the term value in the center of the slit given a unit weight of 1, while those on either side of the center are weighted sequentially less according to their distance from the center. Each transition band is plotted before proceeding with calculations on the next band. All bands around a given laser probe frequency (see Figs.

(III-2(a-d)), laser frequencies indicated by arrows) are normalized (to an arbitrary set of units). Relative amplitudes cannot be obtained between <u>different</u> groups, but only <u>within</u> each group. In Figs. (III-2(a-d)) the simulation bands all degrade to the red with no distinction between P and R branches. Given the average rotational constant B - 0.04 cm $^{-1}$, it is possible to calculate the separation of the P and R branch peaks. The separation is given by;

$$f_{PR}^{MAX} = (2BkT/(hc))^{1/2} = 2.358(BT)^{1/2} \qquad (A15)$$

at 300 K, $f_{PR}^{MAX} = 8.2$ cm^{-1}, indicating that for this simulation the P and R branches will be unresolved. In HgBr, calculations show that $B_{v'} < B_{v''}$[10], therefore the band head is expected to form in the R branch (short wavelength side of the origin) and degrades toward the red. The separation of the origin and band head can be calculated, and for an average band transition it is only 0.13 cm^{-1}. So it is expected that the origin will essentially be the band head.

The simulations in Fig. (III-2) were tested at different rotational temperatures (T_R = ±150 K around 300 K) and it was found that the band shapes had only

slight dependence with T_R. Also tested were the number of rotational levels which are summed over. At a given temperature, the band shapes are quite sensitive to the number of J levels used, but summing greater than 100 rotational levels showed no appreciable change in the curves. All curves in Fig. (III-2) are generated by summing 120 rotational levels at 300 K.

<u>Appendix B:</u> <u>Mapping of nascent v' level population in HgBr($B^2\Sigma^+_{1/2}$) onto v'' states of HgBr($X^2\Sigma^+_{1/2}$).</u>

The nascent v' population distribution in HgBr(B) are derived from calculations by Cool et al.[25] The synthesized distribution is shown in Fig. (III-B1). Also known are the Franck-Condon factors for the various v'—>v'' transitions.[10] Following B—>X emission, the population distribution in the ground ($X^2\Sigma^+_{1/2}$) manifold can be calculated by using the following equations.

$$I_{em}^{v'v''} = N_{v'}A_{v'v''}(h c \nu_{v'v''}) \qquad (B1)$$

$$f(v'') = \sum_{v'} f(v')\, A_{v'v''} \qquad (B2)$$

$$A_{v'v''} = (\nu_{v'v''})^3 R_e^2 |\langle v' | v'' \rangle|^2 \qquad (B3)$$

$$f(v'') = \sum_{v'} f(v')(\nu_{v'v''})^3 R_e^2 |\langle v' | v'' \rangle|^2 \qquad (B4)$$

where Eq. (B1) describes the emission intensity for a single v'—>v'' transition. $N_{v'}$ is the population in level v', $A_{v'v''}$ is the Einstein A coefficient for the transition and $\nu_{v'v''}$ is the transition frequency. For a given v' state population distribution such as f(v'),

FIG. (III-B1). Nascent vibrational distribution for the $B^2\Sigma^+_{1/2}$ state of HgBr follwing 193 nm photolysis of $HgBr_2$. The distribution includes processes where both $Br(^2P_{1/2})$ and $Br(^2P_{3/2})$ are produced. The curve is taken from Reference (25).

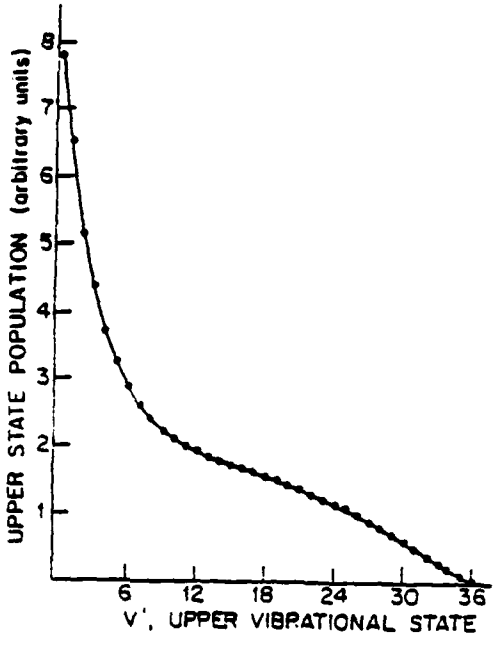

the ground state population distribution $f(v'')$ is generated via a mapping given by Eq. (B2). Equation (B3) shows the relationship of $A_{v'v''}$ to the transition moment and Franck-Condon factor. Inserting Eq. (B3) into Eq. (B2), one gets Eq. (B4) which relates the ground state distribution $f(v'')$ to the various parameters. Knowing the Franck-Condon factors, $f(v'')$ can be calculated to within a constant by summing over the contributions from <u>all</u> v' states. Furthermore, each contribution must be multiplied by $(\nu_{v'v''})^3$ transition frequency.

In the calculation of $f(v'')$ for HgBr(X), the first order approximation was to only consider a number of v' states about the maximum transition overlap integral, $|\langle v'|v''\rangle|^2_{max}$ for a given v'' ground state. A sum of 6 v' states about $|\langle v'|v''\rangle|^2_{max}$ gives a net transition probability which is within 15% of the true total transition probability (summing over all v' for a given v''). Since nearly 85% of the transition probability to a given v'' state comes from a few nearby states about some v', one can also expect that $(\nu_{v'v''})^3$ variation to also be small. An analysis revealed that $(\nu_{v'v''})^3$ variation to be less than 5% for a given v''. To first order, one can simlify Eq. (B4) and make it more

amenable to calculation.

$$f(v'') \approx \sum_{v'=v'_j}^{v'_i} f(v') \, |\langle v'|v''\rangle|^2 \qquad \text{(B5)}$$

Table (III-B1) lists the normalized $f(v'')$ distribution using the digitized values of the nascent distribution in $B^2\Sigma^+_{1/2}$. The $f(v'')$ distribution in the table are for $22<v''<49$. A complete $f(v'')$ for all v'' was not necessary in analyzing the experimental results of Chapter III.

TABLE (III-B1). The normalized $X^2\Sigma^+_{1/2}$ ground state nascent v'' population distribution $f(v'')$.

Selected v''	$f(v'')$
22	1.0
23	0.93
24	0.90
25	0.85
26	0.80
27	0.77
28	0.73
29	0.67
30	0.64
31	0.62
32	0.57
33	0.55
34	0.51
35	0.49
36	0.46
37	0.44
38	0.39
41	0.21
49	0.07

Appendix C: The calculation of HgBr restoring forces and the forces experienced during HgBr+M collisions. The classical approach.

Using equations for the classical harmonic oscillator, a figure for the restoring force can be obtained within an order of magnitude. The force constant for a harmonic oscillator may be determined from the equation.

$$k = 4\pi^2\mu(\nu_{osc})^2 \qquad (C1)$$

where μ is the reduced mass (57.75 au for HgBr)[2] and ν_{osc}, the vibrational frequency. For the anharmonic oscillator HgBr, the vibrational frequency in the state v^* according to classical theory is given by.[2]

$$\nu_{osc} = c\Delta G_{v^*} \qquad (C2)$$

$$\nu_{osc} = c[(\omega_e - \omega_e x_e) - 2\omega_e x_e v^*] \qquad (C3)$$

where ω_e and $\omega_e x_e$ are the known spectroscopic constants. At $v^*=22$, the vibrational frequency $\nu_{osc}(v^*=22)$ is equal to $c(142\ cm^{-1})$ giving a vibrational spring constant k of 6.84×10^4 dyne/cm. In HgBr(X,v^*) the maximum restoring force occurs when the molecule is at the classical turning points. Using the above Equations, the maximum restoring force F for HgBr(X,$v^*=22$) is 4×10^{-4} dyne. To

make a transition between v^* states a smaller perturbation force may only be necessary.

To calculate the forces that might be experienced during a HgBr+M collision usually requires understanding of the collision dynamics and the interaction potential. Here, the classical ball and spring analogy is used to just get a general "feel" for the interaction force. For a given translational energy the classical collision will convert this translational energy of the M_1 species to potential energy in the "coiled" spring (harmonic oscillator HgBr). The restoring force of the perturbed spring will define the force of the collision. This assumption assumes a non adiabatic collision, one which is impulsive. In an adiabatic collision the oscillator spring has time to accomodate itself to the collision and energy transfer becomes inefficient.[26]

At 333 K (experimental temperature) the average translational energy is 233 cm^{-1} (4.6×10^{-14} ergs). The potential energy for a harmonic oscillator is given as;

$$V = 1/2kx^2 \qquad (C4)$$

Setting the potential energy V equal to the translational energy of the M species (233 cm^{-1}) gives a perturbation displacement of $x=0.12\times10^{-8}$cm in the idealized HgBr oscillator. With this displacement, the

generated force F equals 8×10^{-5} dyne. This force is comparable to the restoring force of the HgBr(X,v^*) molecule at $v^*=22$. The calculations of Cool et al., on the classical turning points for HgBr, show that a perturbation displacement of 0.1×10^{-8} cm for v^* levels near $v^*=22$, result in a change of state equaling one vibrational level.

Reference (Chapter III)

[1] E.J. Schimitschek, J.E. Celto, J.A. Trias, Appl. Phys. Lett. 11, 608 (1977).

[2] G. Herberg, Molecular Spectra and Molecular Structure: I. Spectra of Diatomic Molecules (Van Nostrand, New York, 1950).

[3] R.M. Sarc, P.J. Dagdigian, Science 185, 739 (1974).

[4] J.E. Velasco, J.E. Kolts, D.W. Setser, J. Chem. Phys. 69, 4357 (1978).

[5] The chamber is a modification of the the design by J. Campbell. J.D. Campbell, M.E. Yu, C. Wittig, Appl. Phys. Lett. 32, 413 (1978).

[6] P.A. Schweitzer, Corrosion Resistance Tables, Marcel Dekker Inc., New York.

[7] After installing the gated PMT, experiments could be conducted at 338 K and still get sufficient signal intensity, prior experiments required a higher $HgBr_2$ density.

[8] R. Weast, ed., Handbook of Chemistry and Physics (Chemical Rubber Co., Cleveland, 1973).

[9] I. Kovacs, Rotational Structure in Spectra of Diatomic Molecules (American Elsevier, New York, 1969).

[10]Mai-Se Cheung, T.A. Cool, J. Quant. Spectrosc. Radiat. Transfer 21, 397 (1979).

[11]M. Ogawa, J. Chem. Phys. 54, 2558 (1971).

[12]J.O Hirschfelder, C.F. Curtiss, R.B. Bird, Molecular Theory of Gases and Liquids (John Wiley & Sons, Inc., New York, 1954).

[13]A. Dalgarno, Adv. Phys. 2, 281 (1962).

[14]W.R. Wadt, Appl. Phys. Lett. 34, 658 (1979).

[15]K.L. Bell, A. Dalgarno, A.E. Kingston, J. Chem. Phys. B 1, 18 (1968).

[16] K. Liu, J.M. Parson, J. Chem. Phys. 63, 815 (1976).

[17]B.L. Earl, R.R. Herm, J. Chem. Phys. 60, 4368 (1974).

[18]J.R. Barker, R.E Weston, Jr., J. Chem. Phys. 65, 1427 (1976).

[19]S.L. Kramer, D.R. Herschbach, J. Chem. Phys. 53, 2792 (1970).

[20]F. London, Trans. Faraday Soc. 33, 8 (1937).

[21]J.C. Slater, J.G. Kirkwood, Phys. Rev. 37, 682 (1931).

[22]To a first approximation, the polarizability of HgBr was taken to be equal to the HgBr volume (assuming a radius r=2.5x10^{-8} cm). Polarizability of Hg(6^3P_1) in the literature is assumed to be 20x10^{-24} cm^3. S.D. Gleditsch, J.V. Michael, J. Chem. Phys. 79, 409 (1975).

[23]W.J. Wiegand, Investigation of Discharge Processes in Electronically Excited Blue/Green Laseral Final Report (United Technologies Research Center, Conn, July 31, 1980).

[24]T.A. Cool, (unpublished).

[25]J.A. McGarvey, Jr., Mai-Se Cheung, A.C. Erlandson, T.A. Cool, J. Chem. Phys. 74, 5133 (1981).

[26]R.D. Levine, R.B. Bernstein, Molecular Reaction Dynamics (Oxford University Press, New York, 1974).

CHAPTER IV

ENERGY TRANSFER FROM Hg(6^3P_0) TO HgBr($X^2\Sigma^+_{1/2}$)

Introduction

In light of all recent advances in the chemistry of electronically excited atoms,[1] there has been considerable research in the collisional quenching of excited metal atoms.[2] Most previous studies, and rightly so, have focussed on the reactive and energy transfer pathways among interacting atoms and molecules.[3] There have been fewer efforts in investigating interactions between atoms and radicals. The inherent potential in radicals for reactivity makes them suitable candidates for studies in energy transfer, but the difficulties associated with producing and handling them makes such experiments come under stricter scrutiny.

In this chapter, experimental results are presented wherein the deactivation rate of metastable Hg(6^3P_0) by the radical species HgBr(X) is measured. The

deactivation of Hg($^3P_0$) is monitored by chemiluminescence of HgBr(B) via the reactions,

$$Hg(^3P_0) + HgBr(X) \xrightarrow{k_1} Hg(^1S_0) + HgBr(B) \quad (1)$$

$$HgBr(B) \xrightarrow{A} HgBr(X) + h\nu \quad (2)$$

As written, reaction (1) is an exoergic process with its energy transfer and reactive pathways being indistinguishable. Equation (1) also shows only one deactivation pathway from a possible multitude. In Fig. (IV-1), an energy level diagram is drawn to show various product energy states. Reaction (1) is thought to be of importance because (1) it reflects an interaction potential surface upon which energy transfer or reaction may take place; (2) correlation diagrams in (J,Ω) coupling does not seem to restrict or disallow the reaction (3) and in application, the metastable nature of the excited atom, Hg($^3P_0$) can serve as an energy reservoir for the well known mercury-halide HgBr(B-->X) lasers. Reaction (1) has been observed for the Chloride by Vikis & LeRoy,[4] but its rate was never measured. In this chapter, the experimental results can only place an upper limit to the reaction rate in Equation (1). But with the use of correlation diagrams in conjunction with

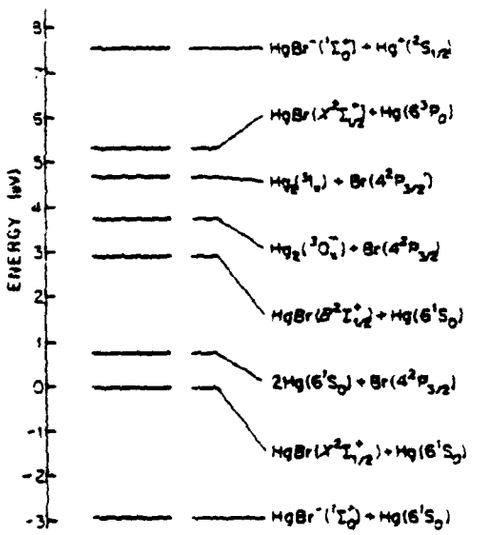

FIG. (IV-1). Energy level diagram for product states which are energetically accessible to the interacting pair $Hg(6^3P_0)$ and $HgBr(X^2\Sigma^+_{1/2})$. Zero energy corresponds to the ground state species $Hg(6^1P_0)$ and $HgBr(X^2\Sigma^+_{1/2})$. The ion pair $Hg^+(^2S_{1/2})$, $HgBr^-(^1\Sigma^+_0)$ is also shown, since the potential surface for this ion pair crosses the surfaces which connect neutral species at the separation associated with the harpoon mechanism (see text for details).

an approximate model for charge transfer,[5] a qualitative understanding of the deactivation mechanism can be presented. The use of correlation diagrams also facilitates a discussion of the importance of other competing quenching processes.

Experimental

The experimental approach is shown schematically in fig. (IV-2). Briefly, in a chamber containing Hg and $HgBr_2$, an ArF laser (193 nm) is used to photolyse $HgBr_2$ vapor producing a known quantity of HgBr(B)[6] which in turn decays (23 ns)[7-9] to HgBr(X). A second pulsed laser, appropriately delayed, is tuned to 253.7 nm $6^1S_0 - 6^3P_1$ Hg resonance transition. HgBr(X) will also absorb 253.7 nm[10] but the cross section for resonant absorption in Hg is 3 orders of magnitude larger.[11] Nitrogen gas is used to quench the 6^3P_1 Hg state to yield the 6^3P_0 Hg metastable.[12] The N_2 density used in the experiment is insufficient to quench HgBr(B).[9] The deactivation of $Hg(6^3P_0)$ is monitored by chemiluminescence of HgBr(B→X) as per reactions (1) and (2); while the deactivation rate coefficient is measured by varying the $HgBr_2$ concentration and

FIG. (IV-2). Schematic drawing of the experimental arrangement. Six thermocouples (not shown) are fixed to different parts of the sample cell in order to monitor the temperature and its uniformity. The temperature could be controlled to ± 1 K for long periods of time. Both 532 and 253.7 nm lasers are spatially filtered and collimated prior to entering the chamber, and a narrow bandpass interference filter (10 nm fwhm) is used to protect the PMT from scattered 532 nm radiation. The 532 nm laser is blocked for those experiments where Br_2 photolysis is not needed.

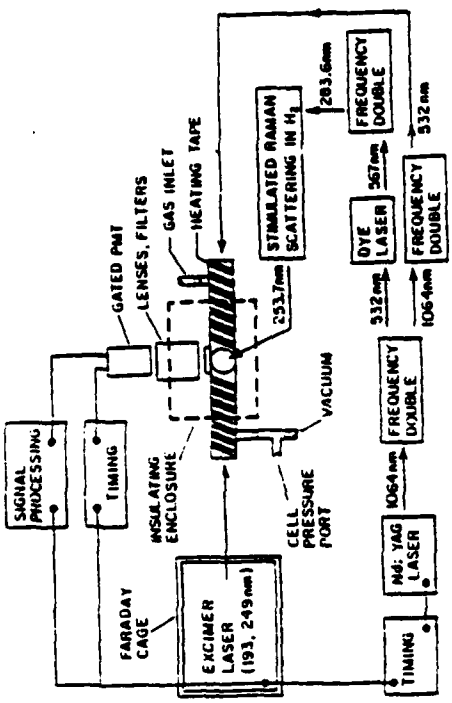

maintaining the Hg concentration constant. The 532 nm radiation shown in Fig. (IV-2) is blocked in this experiment.

The sample chamber resembles a previous design (Chapter III) but is completely made of Pyrex glass with windows mounted using O ring seals. A Pyrex chamber is resistant to most reagents and can be designed to have reasonable temperature stability. Prior to use, the chamber was baked at 300°C to insure that all volatile compounds are removed. It is also externally painted black and completely wrapped with heating tape. Five separate heating tapes were actually used to individually adjust the heat at various places on the chamber. Also a set of six thermocouples are strategically placed in the chamber to monitor temperature uniformity. To further minimize condensation on the windows, the arms and windows are always kept at a temperature which is higher than in the observation region.

The output from the ArF laser (Lumonics, 50mJ) enters the chamber unfocussed through Suprasil quartz windows. After a preset delay, a tuned doubled Nd:YAG pumped dye laser (Quanta Ray, Rhodamine 590, 25 mJ, 10 ns fwhm) is frequency upconverted (X2 KDP, Raman

Shifting in H_2, 1st anti-Stokes) and enters the chamber crossing the ArF laser at right angles. Both lasers enter and leave the chamber through long arms which minimizes scattered laser light. Chemiluminescence is observed at right angles to both lasers through a telescope/filter/gated PMT (EMI, 9659QB, 165-900 nm, 10 ns) arrangement. Signals from the PMT are digitized and averaged (Biomation, 10 ns gate/Tracor Northern) until adequate signal to noise is obtained. Fig. (IV-3) shows a typical signal plotted over several exponential lifetimes. To characterize the signal and insure that the emission is HgBr(B-->X) as per Equations (1) and (2), a set of narrow band filters were used to check the spectral nature. The observed emission was solely between 350-500 nm with a peak near 500 nm. This broad emission band is well known to be HgBr(B-->X)[13] (see Fig. (I-1)). Furthermore, no emission could be observed when either Hg or N_2 was absent from the cell, or when the 253.7 nm excitation laser was detuned from the Hg resonance transition. The emission is only observed when both photolysis and 253.7 nm excitation lasers are used in the proper sequence.

In preparation and prior to the experiment, purified mercury was first transferred into the chamber

FIG. (IV-3). Typical data from the transient digitizer/signal averager combination. The time scale origin is coincident with the 8 ns 253.7 nm laser, and the 1 us delay is required in order to gate the PMT completely on following excimer laser photolysis. For the case shown, the pressures of $HgBr_2$ and N_2 were 5 mTorr and 125 mTorr respectively. The results are an average of 256 laser firings, and four or five such rates are averaged to obtain the deactivation rate at one temperature (see Fig. (IV-4)).

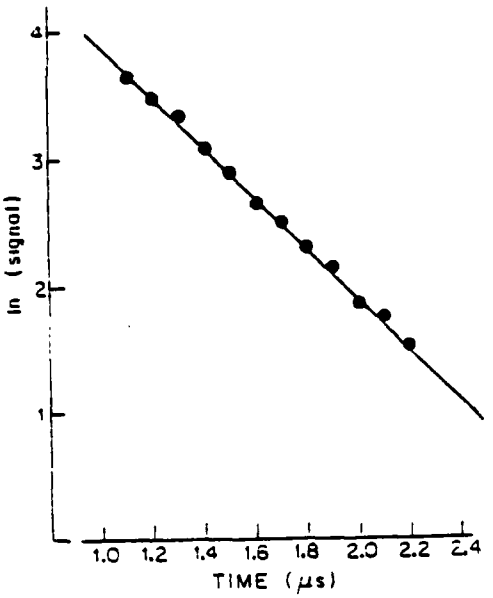

at a known temperature (310 K, [Hg] - 1.5×10^{14}cm^{-3}).[14] The chamber was allowed to cool and a few milligrams of $HgBr_2$ was then placed inside, the chamber was pumped out, then filled with 150 Torr of purified N_2 and sealed. All further experiments conducted were at temperatures whereby the Hg concentration is kept constant. $HgBr_2$ has a reasonable vapor pressure at modest temperatures (100 mTorr at 373 K). The concentration of $HgBr_2$ throughout the experiment was solely derived from temperature versus vapor pressure curves (see Table (II-1)). Diffusion of species from the observation region is expected to have negligible effect given the experimental conditions.[15]

Results

Equations (1) and (2) indicate two possible channels from the various deactivation paths open to the metastable $Hg(^3P_0)$ and the electronically excited radical HgBr(B). In this experiment, quenching of the excited radical, by various photofragments can be neglected because of the short $B^2\Sigma^+_{1/2}$ state lifetime (23 ns) and the low number densities involved. Nitrogen, the species in largest concentration is known

to be an inefficient quencher of both HgBr(B) and $Hg(^3P_0)$. Thus, HgBr(B) deactivation is strictly governed by spontaneous emission. Quenching of the metastable Hg by undissociated parent molecules ($HgBr_2$) contributes only a very small amount to the observed quenching, because of the high quantum efficiency of photodissociating $HgBr_2$ (QE - 1.0 at 193 nm).[16] With nearly 100% dissociation yields, the concentration of $HgBr_2$ in the observation region is expected to be small. This was experimentally verified by measuring no change in the initial photolysis HgBr(B-->X) emission intensity with variation in ArF laser energy. However, HgBr(X) species can react with Br atoms to form Br_2 molecules. Since both HgBr(X) and Br are in equal concentration the removal of HgBr(X) with Br will be second order with respect to [HgBr(X)]. The rate coefficient for such a reaction is not known, but the reaction is clearly exothermic. An LIF experiment was conducted to probe for Br_2, and given the experimental conditions no LIF emission could be observed. With the aforementioned, listed below are the relevant kinetic processes in addition to those of Equations (1) and (2).

$$Hg(^3P_0) + HgBr(X) \xrightarrow{k_3} \text{All other quenching processes} \quad (3)$$

$$Hg(^3P_0) + Br(^2P_{1/2,3/2}) \xrightarrow{k_4} Hg(^1S_0) + Br(^2P_{1/2,3/2}) \quad (4)$$

$$Hg(^3P_0) + Hg(^1S_0) \xrightarrow{k_5} Hg(^1S_0) + Hg(^1S_0) \quad (5)$$

one solution to these equations (Eqs. 1-5) is the time behavior of the radical HgBr(B) number density. It has the general form,

$$[HgBr(B)](t) = C[e^{-\alpha t} - e^{-At}] \quad (6)$$

where α, A and C are constants with A being the spontaneous emission rate of Equation (2). Under the experimental conditions $A >> \alpha$ and by delaying data acquisition a few hundred nanoseconds, the solution simplifies to a sensible single exponential of the form,

$$[HgBr(B)](t) = Ce^{-\alpha t} \quad (7)$$

$$\alpha = (k_1+k_3)[HgBr(X)] + k_4[Br(^2P)] + k_5[Hg(^1S_0)] \quad (8)$$

where the exponential behavior now reflects the net deactivation of the $Hg(^3P_0)$ metastable. The time constant α at a particular temperature is obtained by simply plotting the ln([HgBr(B)]) versus time (Fig. IV-3)). The definition for α can be simplified by noting that HgBr(X) and $Br(^2P)$, both products of $HgBr_2$ photolysis, have equal concentrations for a given temperature. Since the Hg density is kept constant, a

plot of a versus [HgBr(X)] should be linear having a slope equal to the sum rates $k_1+k_3+k_4$ as shown in Fig. (IV-4). The measured value of this slope was $(2.7\pm0.4)\times10^{-9}cm^3molec^{-1}s^{-1}$. To establish the rate coefficient for the deactivation of $Hg(^3P_0)$ by HgBr(X), or k_1+k_3, it is necessary to know k_4. From a separate independent experiment the deactivation rate of $Hg(^3P_0)$ by $Br(^2P)$ atoms was established (see Appendix A for summary of experiment and results). The measured rate coefficient is $(1.0\pm0.34)\times10^{-9}cm^3molec^{-1}s^{-1}$. By substracting k_4 from the slope in Fig. (IV-4), the rate coefficient k_1+k_3 for the deactivation of $Hg(^3P_0)$ by HgBr(X) equals $(1.7\pm0.83)\times10^{-9}cm^3molec^{-1}s^{-1}$. It is surprising that even after allowing for experimental errors, the resulting rate coefficient k_1+k_3 is still large, much larger than the gas kinetic quenching rates. It seems only obvious to claim that long range interaction forces are in effect, though the simple dipole-dipole interaction should not be the major coupling mechanism. The dipole-dipole interaction, also termed "Golden Rule" quenching (termed as such, because the quenching rate is derived from the Fermi Golden Rule Equation),[17] would be expected for dipole transitions which are fully allowed. Since the Hg

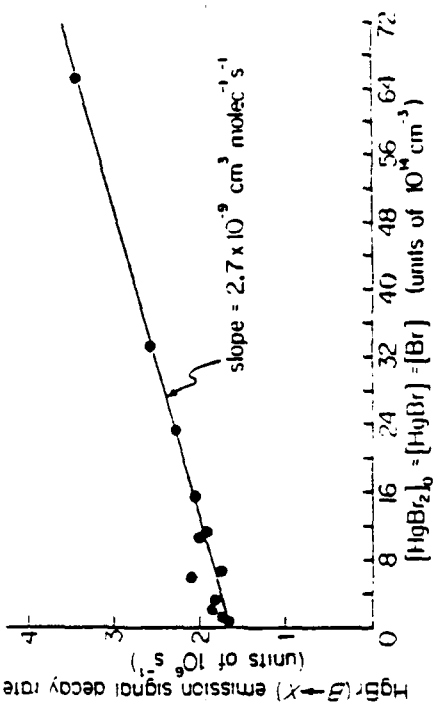

FIG. (IV-4). $Hg(^3P_0)$ deexcitation rate vs. $[HgBr_2]_0$. Each point represents an average of 1024 fluorescence traces. The straight line is a least squares fit.

6^3P_0-6^1S_0 transition dipole is vanishingly small, a "Golden Rule" type quenching has small probability. The well known "harpoon" charge transfer coupling scheme, whereby exit channels are reached through the intermediacy of an atom-to-quencher charge transfer state, may be applicable here, since charge transfer interactions can occur at relatively long range.

Discussion

It is appropriate at this point to mention that any general quenching mechanism employed can only provide a qualitative description. There has been no quantitative attempt made to apply detailed energy transfer theories to $Hg(^3P_0)$ and HgBr(X). One must be satisfied with descriptions which are physically reliable under approximations.

One of the complexities associated with the collisional behavior of heavy atoms is that any symmetry arguments employing the weak spin orbit coupling approximation does not clearly present the right chemistry. Quenching studies on Hg (spin orbit splitting - 0.2 eV) should be discussed in terms of symmetry arguments based on (J,Ω) coupling, the more

suitable vehicle when considering chemistry of heavy atoms.[18] To this end, the quenching molecule HgBr(X) must also be considered using (J,Ω) coupling arguments. Relaxation of the spin quantum number often results in there being a large number of non-degenerate surfaces correlating reactant species to various product states. Therefore, there may be many possible surface crossings, characterized by high transition probabilities, and hence the absence of direct adiabatic pathways maybe circumvented via diabatic channels leading to those products of interest. Ideally, correlation diagrams based on (J,Ω) coupling should include the effect of rotation on the appropriate Hund's coupling cases for the molecule in concern. In this analysis, it is the intention to only provide a qualitative understanding and perhaps show the existence of any obvious barrier which may keep the reactants from correlating to specific products of interest. Thus, the correlation diagrams presented utilize (J,Ω) coupling[19] but neglect rotational effects. Figures (IV-5) and (IV-6) show these correlation diagrams. Only those surfaces which directly connect the reactants to products are drawn. (see Appendix B for the analysis of both (L,S) and (JΩ) coupling schemes). Two collision trajectories have been

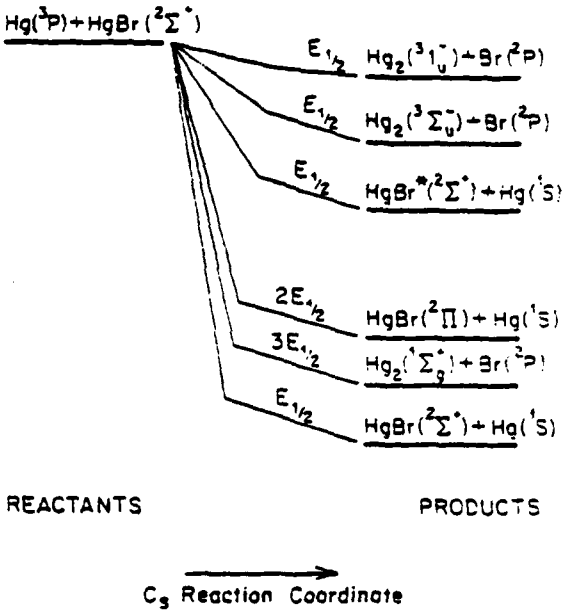

FIG. (IV-5). Correlation diagram in (J,Ω) coupling connecting the reactants Hg(^{3}P) and HgBr($^2\Sigma^+$) to various possible products. In this diagram, the correlation is assumed to go through a HgBrHg intermediate of C_s symmetry.

FIG. (IV-6). Correlation diagram in (J,Ω) coupling connecting the reactants Hg(^{3}P) and HgBr($^2\Sigma^+$) to various possible products. In this diagram, the correlation is assumed to go through a HgBrHg intermediate of $C_{\infty v}$ symmetry.

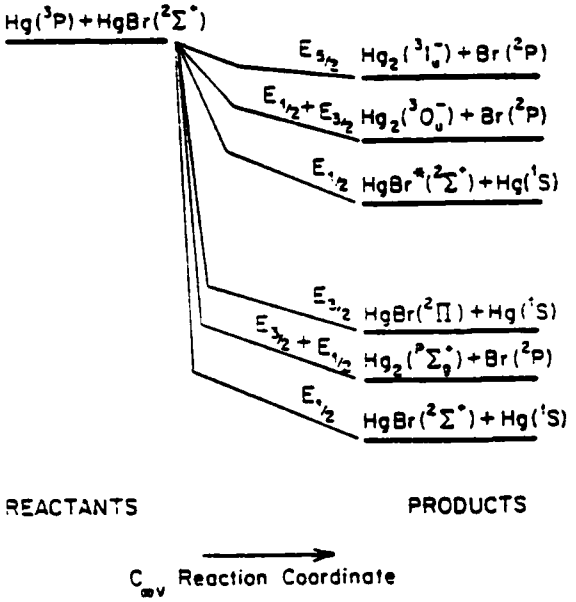

considered, the end-on approach leading to a $C_{\infty v}$ triatomic intermediate and the side-on collision leading to an intermediate having C_s symmetry. Since the radical HgBr(X) is expected to be rotating, a collision along a C_s reaction path is more likely. But based on dynamical arguments, a $C_{\infty v}$ reaction path where the excited $Hg(^3P_0)$ approaches the radical HgBr(X) from the bromine side is more likely to lead to reaction and production of excited HgBr(B) species.

Both collision trajectories show that adiabatic pathways exist which lead to the production of electronically excited mercury excimers $Hg_2(^3\Pi_u)$ and $Hg_2(^3O_u^-)$. The $Hg_2(^3\Pi_u)$ excimer which lies ~ 1eV above the $Hg_2(^3O_u^-)$ potential well[20] requires a third body to be collisionally stabilized.[21] The departing Br atom can serve to remove excess energy and stabilize either excimer pair. Both excimers have fluorescent bands, the $Hg_2(^3\Pi_u) \rightarrow Hg_2(^1\Sigma_g^+)$ emission at 335.0 nm and the $Hg_2(^3O_u^-) \rightarrow Hg_2(^1\Sigma_g^+)$ band at 485.0 nm.[20-21] These emission bands do happen to be in the spectral region where the HgBr(B→X) emission signal is monitored. However, the excimer decay lifetimes, under the experimental conditions are in the ~ ms range[20-21] and much larger than the HgBr(B→X) lifetime of 23 ns.

Emission intensities from the excited mercury excimer states are expected to be small because of the metastable nature of the excited state. Though mercury excimer emission was not observed, one must consider that Hg_2 excimer formation is a possible product species in the deactivation of $Hg(^3P_0)$ by the radical species HgBr(X). It should be noted that all channels which lead to the formation of the products $Hg_2(^1\Sigma_g^+)$ and $HgBr(^2\Pi)$ will eventually lead to dissociation of the diatomic product species. Both $Hg_2(^1\Sigma_g^+)$ and $HgBr(^2\Pi)$ have repulsive potentials which correlate to ground state atoms. Since a number of adiabatic correlations can be drawn from the reactants to dissociative products, it is believed that in the deactivation of $Hg(^3P_0)$ by HgBr(X), one salient quenching mechanism is the collision induced dissociation of HgBr(X).

The measured net deactivation rate of $Hg(^3P_0)$ by HgBr(X), within experimental uncertainty, is found to greatly exceed the gas kinetic rate for the colliding pair ($\sigma_{exp} = (690 \pm 550) \times 10^{-16} cm^2$ $\sigma_{HS} = 50 \times 10^{-16} cm^2$).[22] Therefore it becomes necessary to consider alternate quenching mechanisms which allow for long range interaction. One such theory which has had reasonable success is the charge transfer or "harpooning" model.

It has been successfully used to explain the large reaction cross sections for alkali atom reactions with halogens,[23-24] and because of their lowered ionization potentials, the quenching of the ^3P states of Hg and Cd by various molecules.[25-26] It was found that those molecules which proved to be effective quenchers, had electron affinities commensurate with the ionization potential of the colliding atom. The basic premise of the model is that for an excited atom A^* and quenching molecule M, it is possible for a potential surface of predominantly A^+M^- character to cross the diabatic A^*-M interaction surface at distances sufficiently large that the A^*-M curve is sufficiently flat (Fig. (IV-7)). To first order, the curve crossing distance R_{CT} is defined by the Coulomb potential where the energy term is the energy difference between A^*+M and A^++M^- surfaces at infinite A-M distance. Neglecting polarizability of the A^+M^- complex, R_{CT} can be written as,

$$R_{CT} = \frac{e^2}{IP(Hg(^3P_0)) - EA(HgBr(X))} \quad (9)$$

where IP is the ionization potential for $Hg(^3P_0)$ (5.78 eV)[14] and EA is the electron affinity of the radical HgBr(X). From calculations by Krauss et al.,[28]

FIG. (IV-7). Potential energy curves for an atom-atom interacting system. For an atom-molecule case vibrational states for each potential would have to be added. Clearly the crossing points are strongly dependent on the ionic parameters of A^*, the excited atom, and M, the quenching atom, i.e. on the ionization potential of A^*, the electron affinity of M, and the polarizability of the $A^+ + M^-$ intermediate. Figure is taken from Reference (27).

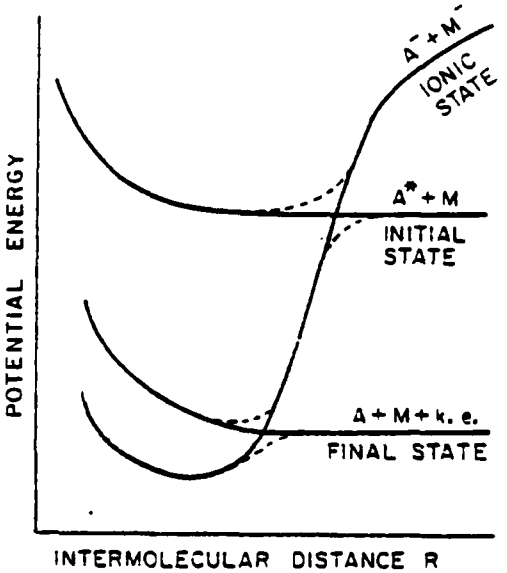

one can estimate the electron affinity for HgBr(X) to be about 2.9 eV (taken from the potential wells of the neutral and negative ion between the minimum points). To first order, the curve crossing distance R_{CT} is 5.0×10^{-8}cm. However, R_{CT} is measured from the center of charge in $HgBr^-$ to the nucleus of $Hg(^3P_0)$, while the hard sphere radius R_{HS} is measured from the center of mass of HgBr to the nucleus of $Hg(^3P_0)$. If one assumes the center of charge as the Br nucleus in HgBr, a factor has to be added to R_{CT} to shift the origin to the HgBr center of mass. Shifting this origin, R_{CT} is normalized to a value of 6.4×10^{-8}cm, giving a charge transfer cross section of $\sigma_{CT} = 129\times10^{-16}cm^2$. This is larger than the hard sphere cross section ($\sigma_{HS} = 50\times10^{-16}cm^2$) implying that the charge transfer curve crossing, and hence quenching, can occur prior to the hard sphere $Hg(^3P_0)$ - HgBr(X) collision radii. However, σ_{CT} is still smaller than the experimentally measured reaction cross section ($\sigma_{exp} = (690\pm550)\times10^{-16}cm^2$). This apparent difference may be accounted if we consider the previous studies on alkali-halogen molecule reactions. In that investigation, it was found that the reactive scattering cross sections are determined by an impact parameter for orbiting[17] in the perturbed entrance

potential. If this orbiting impact parameter (the radii at which the centrifugal barrier is located for the given kinetic energy E) is greater than the charge transfer radii, the criteria for reaction is surmounting the centrifugal barrier, i.e., after crossing the barrier, electron transfer occurs with unit probability.[17] Therefore, the quenching cross section is governed by the orbiting model.[29,30] In the case of the alkali-halogen molecule reactions, numerical solutions of the relevant equations place the centrifugal barrier - 2×10^{-8}cm outside the diabatic (charge transfer) crossing radius.[5,30] In the $Hg(^3P_0)$ - HgBr(X) system, an accurate and meaningful calculation of the orbiting radius would require estimating several parameters with high confidence. Lacking such precision in the parameters an orbit controlled charge transfer quenching cannot be ruled out. However, the charge transfer coupling is considered an important aspect of the interaction. For charge transfer to occur, the oncoming $Hg(^3P_0)$ atom must be in the vicinity of the Br atom. In other words, for efficient charge transfer, $Hg(^3P_0)$ should attack HgBr(X) from the Br end. This dynamical constraint was also apparent in the alkali-halogen molecule studies.[30] In the $Hg(^3P_0)$ - HgBr(X)

experiment any collision in which the two Hg atoms come near, may lead to a covalent type quenching, excimer formation or repulsion. While an interaction between $Hg(^3P_0)$ - BrHg may lead to charge transfer followed by either HgBr(B) formation (HgBr(B) state has ionic character, especially for high v' states) or HgBr(A) formation which is repulsive and leads to ground state atoms. This possibility is viable because at high energies, the HgBr(A) and HgBr(B) potential curves are known to cross. The interaction may initially form vibrationally excited HgBr(B; v' - 25-30) species but curve cross to the repulsive HgBr(A) potential. A third option with the $Hg(^3P_0)$ - BrHg approach is stable HgBr(X) production. This situation is indistinguishable between simple quenching or reactive (charge transfer) interaction with ground state products. The latter possibility is expected to have a low probability of occurrence. HgBr(X) has a low potential well (0.7 eV) which would leave in excess of 4.0 eV to be partitioned as relative translation between Hg and HgBr. The outcome of the charge transfer reaction could also be influenced by the approximity of the spectator Hg atom.[31]

Although the net deactivation rate of $Hg(^3P_0)$ by HgBr(X) is truly the aggregate effect of numerous

quenching mechanisms, it is believed that the charge transfer mechanism or the orbit controlled charge transfer mechanism are the most important quenching processes.

The measured net deactivation rate coefficient k at best is an upper limit for the rate of Reaction (1), but in view of the correlation diagrams with the multitude of possible products, the production of excited HgBr(B) from quenching of $Hg(^3P_0)$ by HgBr(X) is thought to be a minor channel. It is annoying that the deactivation rates k_1 and k_4 could not be measured with higher precision. Both experiments were very difficult and besides the experimental sophistication required to obtain higher precision would supersede the net gain in physical insight.

Appendix A: Measurement of the rate coefficient for the deactivation of metastable $Hg(6^3P_0)$ by atomic $Br(4^2P_{1/2,3/2})$.

In general, it is well known that atomic species in electronically excited states are quenched efficiently by molecular gases while as quenchers, most atomic gases appear to be rather inefficient.[32] This general behavior has been attributed to the efficiency of energy transfer from electronic to vibrational modes of molecules in comparison to the poorer coupling between electronic and translational energies. However, there have been quenching experiments where deactivation cross sections were noticably greater than simple hard sphere collision cross sections.[3,33] These results could not be easily explained via covalent type atom-molecule or atom-atom interactions. Alternate quenching mechanisms which allow for long range interaction have been utilized, but for reactions where one species has a low ionization potential while the other a commensurate electron affinity, the charge transfer theory or "harpooning" model has been especially reliable in

providing a qualitative description of the reaction dynamics.[17]

In this Appendix, results are discussed wherein the deactivation of metastable $Hg(^3P_0)$ by $Br(^2P)$ atoms is measured. The results from this experiment also provide the rate coefficient which is necessary in reducing those results of Chapter IV. The reaction of interest can be written by the equation.

$$Hg(6^3P_0) + Br(4^2P_{1/2,3/2}) \xrightarrow{k'} Hg(6^1S_0) + Br(4^2P_{1/2,3/2}) \qquad (A1)$$

The mercury and bromine atoms are prepared from separate photolysis reactions, while the excitation of Hg is via resonance absorption. The net deactivation of $Hg(^3P_0)$ is monitored by the chemiluminescence of HgBr(B) via the reactions,

$$Hg(^3P_0) + Br_2 \xrightarrow{k} HgBr(B) + Br(^2P_{1/2,3/2}) \qquad (A2)$$

$$HgBr(B) \xrightarrow{A} HgBr(X) + h\nu \qquad (A3)$$

where k is a known rate constant and A is the Einstein A coefficient for HgBr(B-->X).

The quenching in Equation (A1) is simple E-T (electronic to translational) energy transfer. It is

also the only deactivation path available to the $Hg(^3P_0)$ - Br collision pair. There are no bromine electronic states nearby to allow efficient resonant E-E (electronic-electronic) energy transfer.[34] Mercury in its ^3P state has a lowered ionization potential and it is expected that the metastable state will resemble a ground state alkali atom in its chemical properties. The "harpoon" mechanism as explained in Chapter IV is expected to be the dominant quenching mechanism.

The experimental approach is shown schematically in Fig. (IV-2), but for this experiment it contains a small amount of $HgBr_2$ salt and Br_2. A KrF laser (249 nm) is used to photolyze $HgBr_2$ vapor producing a quantity of Hg atoms. $HgBr_2$ has an absorption cross section of $\sim 2\times10^{-18}cm^2$ at 249 nm and is known to produce Hg atoms with reasonable quantum efficiency.[6,35-36] After an appropriate delay, a second pulsed laser enters the chamber and is turned to the 6^1P_0-6^3P_1 Hg transition at 253.7 nm. This is quickly followed by a third laser at 532 nm which is used to excite Br_2 molecules to predissociative levels of the $Br_2(B^3\Pi_0^+)$ electronic state (τ_{diss} - 260 ns)[37] Nitrogen gas in the chamber ($[N_2] - 4.5\times20^{18}cm^{-3}$) serves to both help quench $Hg(^3P_1)$ to $Hg(^3P_0)$ and to enhance the Br_2 dissociation

measured using an MKS Baratron gauge, while Br atom concentrations were deduced from the Beer-Lambert absorption equation, using known extinction coefficients for Br_2 at 532 nm[40] and the average laser energy (5.9 mJ). At the measured laser energies, only 2.4% of the Br_2 molecules are photolyzed allowing the calculation of [Br] from a Beer-Lambert relationship. Furthermore, the beam waist of the 532 nm laser is kept several times larger than that of the 253.7 nm laser in order to minimize the spatial variation of [Br] in the region where $Hg(^3P_0)$ quenching occurs.

Equations (A2) and (A3) provide a scheme with which to measure the net deactivation rate of $Hg(^3P_0)$ atoms. Both equations have large cross sections ($k \sim 10^{-10}cm^3molec^{-1}s^{-1}$, $A = 4.3\times10^7s^{-1}$) and serve to reliably monitor the $Hg(^3P_0)$ concentration. In the experiment quenching of the excited radical HgBr(B) by various photofragments is neglected, because of the short $B^2\Sigma^+_{1/2}$ state lifetime (23 ns) and the low number densities involved. Nitrogen, the species in large concentration is known to be an inefficient quencher of both HgBr(B) and $Hg(6^3P_0)$, while Br_2 known to readily quench HgBr(B),[9] is of such concentration as to have a negligible effect. Thus, HgBr(B) deactivation is

by collisions (τ_{diss} - 100 ns @ 100 Torr N_2)[38] Optical cross sections of Br_2 at 249 nm and 253.7 nm are known to be small ($\sigma \sim 2\times10^{-21}cm^2$),[39] so there should not be large densities of Br_2 molecules in highly excited states. The net deactivation of $Hg(^3P_0)$ is monitored by the chemiluminescence of HgBr(B-->X) as per reactions (A2) and (A3) with Br_2 concentration held in excess. The deactivation rate coefficient k' in Equation (A1) is deduced by first separately measuring the net $Hg(^3P_0)$ quenching rate in the cases of with/without the Br_2 photolysis laser. The measured change in the rate when plotted against Br_2 atom concentration is proportional to k'.

All data acquisition and diagnostic analysis are as discussed in the text of Chapter IV. In addition the chemiluminescence signal was characterized with the use of narrow band filters, where it could be assured that it was HgBr(B-->X) emission. Furthermore, no chemiluminescence could be observed when either Br_2 was removed from the cell or when the 253.7 nm excitation laser was detuned from the Hg resonance transition. All the experiments were conducted at one temperature (T=40°C; $[HgBr_2] \sim 10^{13}cm^{-3}$)[14] to insure sufficient $HgBr_2$ density. Bromine molecule concentrations were

strictly governed by spontaneous emission (Eq. 'A3)). Though HgBr(B) has but one deactivation pathway, the metastable $Hg(^3P_0)$ can be quenched by enumerable products through a multitude of possible channels. To obtain the specific quenching rate of $Hg(^3P_0)$ by $Br(^2P)$ atoms (Eq. (A1)) from the various quenching processes, one needs to measure the change in the net deactivation rate of $Hg(^3P_0)$ when the $Br(^2P)$ concentration is reduced to zero. If all other species concentrations are kept constant, this difference in the measured rates can be made to only be proportional to the $Br(^2P)$ concentration while other common terms cancel. Since the $Br(^2P)$ concentration is reduced to zero when the Br_2 photolysis laser is off, it is only of importance to check those unwanted products which might be produced via photolysis at 532 nm. All multiphoton processes can be neglected on grounds of low optical cross section, while all absorption processes with products produced by the KrF laser are neglected because of low densities. Thus it is only necessary to consider those Br_2 molecules which are excited by 532 nm radiation but do not predissociate. The $Br_2(B^3\Pi_0^+)$ and $Br_2(A^3\Pi_0^+)$ metastable states are optically coupled to the $Br_2(^1\Sigma_g)$ ground state by emission at 650-900 nm[41-45] with long lifetimes

(A^3 =347μs, B^3 =12.4ms). A careful observation of this spectral region was made and it is believed that given the experimental conditions, the Br_2 metastable concentrations are at best very small. For completeness, one more kinetic equation is necessary in addition to those of Eqs. (A1) - (A3).

$$Hg(6^3P_0) + M \xrightarrow{k_M} \text{All Processes} \qquad (A4)$$

One solution to these equations (Eqs. (A1) - (A4)) is the time behavior of the radical HgBr(B) number density. It has the general form,

$$[HgBr(B)](t) = C(e^{-at} - e^{-At}) \qquad (A5)$$

where a, A, and C are constants with A being the spontaneous emission rate of Equation (A3). In the experiment, A >> a and by delaying data acquisition a few hundred nanoseconds, the solution simplifies to a single exponential of the form,

$$[HgBr(B)](t) = Ce^{-at} \qquad (A6)$$

where a is the net deactivation of the $Hg(6^3P_0)$ metastable. The time constant, a, is obtained by simply plotting ln([HgBr(B)]) versus time. It is defined differently for when the Br_2 photolysis laser is on or

FIG. (IV-A1). $Hg(^3P_0)$ deexcitation rate vs. $[Br_2]_0$. The open circles are for the case of $Hg(^3P_0)$ quenching by Br_2 only and the slope is (least squares fit) 1.2×10^{-10} $cm^3molec^{-1}s^{-1}$. In the case of the darkened circles, $[Br_2]_0$ is partially dissociated with the 532 nm photolysis laser (Fig. (IV-2)), and the quenching of $Hg(^3P_0)$ is due to both Br_2 and Br. The slope is (least squares fit) 1.7×10^{-10} $cm^3molec^{-1}s^{-1}$, and is equal to $(k+f(2k'-k))$, where f is the fraction of $[Br_2]_0$ which is dissociated. Each point is the result of ≥ 2000 laser firings. The largest source of uncertainty derives from not knowing $[Br_2]_0$ accurately enough. Despite a large random error, for a given gas sample, one can see the systematically larger rates in the case of closed circles as compared to the open circles.

off. Without the 532 nm photolysis laser,

$$a_{off} = k[Br_2]_0 + k_M[Hg(^3P_0)] \qquad (A7)$$

and since $k_M[Hg(^3P_0)]$ is constant ($[HgBr_2]$ constant) a plot of a_{off} vs. $[Br_2]_0$ ($[Br_2]_0$ is the Br_2 concentration prior to 532 nm photolysis) gives a straight line with slope $k=(1.2\pm0.1)\times10^{-10}cm^3molec^{-1}s^{-1}$ (see Fig. (IV-A1) open circles) and this is the rate coefficient for the quenching of $Hg(^3P_0)$ by Br_2. Now 532 nm radiation enters the chamber and dissociates a fraction, f, of the Br_2. Under these conditions

$$a_{on} = k[Br_2] + k'[Br] + k_M[Hg(^3P_0)] \qquad (A8)$$

$$a_{on} = (k + f(2k'-k))[Br_2]_0 + k_M[Hg(^3P_0)] \qquad (A9)$$

A plot of a_{on} vs. $[Br_2]_0$ gives a straight line with slope (k+f(2k'-k) (see Fig. (IV-A1) closed circles), and since k has been established and f is known (2.4%), one could obtain k'. The rate coefficient for the deactivation of $Hg(^3P_0)$ by $Br(^2P)$ atoms is deduced to be $(1.0\pm0.4)\times10^{-9}cm^3molec^{-1}s^{-1}$. Because k' is derived from a difference of two measured rates, it can be subjected to large experimental errors. In anticipation of this problem each measured rate was established to a greater degree of accuracy so that the difference rate between them would have sum error that would still be

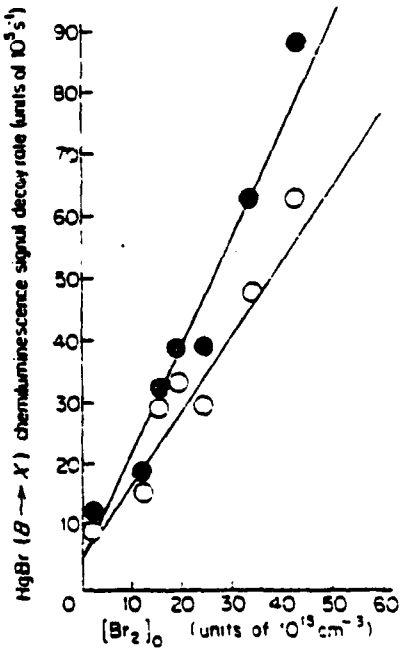

experimentally acceptable. The calculated error also includes an anticipated error of the Br_2 absorption coefficient at 532 nm (actually twice the error mentioned in the reference was used in the error calculations). It is then surprising that after allowing for experimental errors, the resulting rate coefficient k' is larger than gas kinetic quenching rates. The observed large deactivation rate is indicative of coupling forces which have long range interaction. Because the Hg 6^3P_0-6^1S_0 transition dipole is vanishingly small, one could not claim simple dipole-dipole forces to be the major coupling mechanism. By virtue of its excitation, $Hg(^3P_0)$ has a lowered ionization potential, and $Br(^2P)$ an electron affinity of the same magnitude, the "harpoon" model or charge transfer coupling method is most likely to give the best qualitative description of the quenching dynamics. A first order calculation reveals that the charge transfer radius for the $Hg(^3P_0)$-Br pair is at 6.0×10^{-8}cm while the gas kinetic radius is 2.6×10^{-8}cm.

The problem centers in the formulation of the orbit correlation rules.

When considering the simple interaction shown above, it becomes necessary to set up tables which take spherical symmetry (atom A) and diatomic symmetry (BC) to a symmetry X (intermediate ABC). A similar table is compiled which takes the symmetry of atom C and diatomic BA to a symmetry X for ABC. The allowed electronic states of ABC (symmetry X) are then obtained by forming direct products of representations found from the resolution tables (A—>X; BC—>X and also BA—>X and C-> X). The given states of reactants and products will correlate if at least one species arises from the states formed by the reactants and the states formed by the products.

A non linear complex of 3 atoms will belong either in $C_1(C_{\infty v})$, C_s, C_{2v}, and C_{3v}. Consider for example the reaction,

$$Hg(^3P_u) + HgBr(X^2\Sigma^{1/2}{}_{1/2}) \longrightarrow Hg(^1S_g) + HgBr(B^2\Sigma^+{}_{1/2}) \quad (B1)$$

through a non linear complex of C_s symmetry. Utilizing

established tables (Ref. 46) the direct cross products can be written

$$\text{Reactants:}\quad {}^3P_u \times {}^2\Sigma^+ \longrightarrow 2^2A' + {}^2A''$$
$$\longrightarrow 2^4A' + {}^4A''$$
$$\text{Products:}\quad {}^1S_g \times {}^2\Sigma^+ \longrightarrow {}^2A'$$

Thus, the only surface which connects the products with the reactants is the single $^2A'$ surface. If the reaction (B1) is considered through a $C_{\infty v}$ linear complex, the intermediate possible states are given via the following rules.

1. Possible intermediate (L) states resulting
   $M_{L(HgBrHg)} = M_{L(Hg)} + M_{L(HgBr)}$
   $M_{L(Hg)} = L, L-1, \ldots -L \quad (M_{L(Hg)} = 1,0,-1)$
   $M_{L(HgBr)} = \pm\Lambda_d \quad (M_{L(HgBr)} = 0)$
   with $\Lambda_{HgBrHg} = 0,1$
2. Possible intermediate (S) states resulting
   $S_{ik} = S_i+S_k, S_i+S_k-1, \ldots S_i-S_k$ and
   $S_{ik} = S_{HgBrHg} = 3/2, 1/2$

In Table (IV-B1) various product/reactant interaction pairs of concern are correlated to form an intermediate HgBrHg complex of either C_s or $C_{\infty v}$ symmetry. All correlations assume small spin orbit coupling. Figs.

Appendix B: Correlation diagrams, a summary of the necessary sequential operations for adiabatic correlation either via (L,S) coupling (small spin-orbit interaction) or (L,Ω) coupling (large spin-orbit interaction). The formulation is exclusively applied to the case of $Hg(6^3P_0)$ + HgBr(X) species.

The following summary of operations was gleaned from various sources,[46-48] but in the case of (J,Ω) coupling all information was exclusively from the Appendices of Herzberg, Vol. III (Polyatomics).[19] The formulation utilizes group theoretical arguments relating symmetry properties of the reactants, the intermediate reaction complex and the products.

(L,S) Coupling

If spin-orbit coupling is small, spin correlational rules for linear and non linear polyatomics are identical with those for diatomic molecules. The electron spin is not affected by the electric field arising from the interaction of the combining molecules/atoms, and Λ, S, Σ are good quantum numbers.

TABLE (IV-B1). Correlation of various interaction pair to form the intermediate HgBrHg either in C_s or $C_{\infty v}$ symmetry in (L,S) coupling.

Process	C_s intermediate	$C_{\infty v}$ intermediate
$Hg(^3P_g)+HgBr(^2\Sigma^+_{1/2})$	$2^2A'+^2A''$	$^2\Sigma^+_{1/2}$, $^4\Sigma^+_{3/2}$, $^2\Pi_{3/2}$
	$2^4A'+^4A''$	$^4\Pi_{5/2}$
$Hg^+(^2S_{1/2})+HgBr^-(^1\Sigma^+)$	$^2A'$	$^2\Sigma^+_{1/2}$
$Hg_2(^3\Sigma_u)+Br(^2P_u)$	$4^2A'+2^2A''$	$^2\Sigma_{1/2}$, $^4\Sigma_{3/2}$, $^2\Pi_{1/2}$
	$4^4A'+2^4A''$	$^4\Pi_{3/2}$, $^2\Delta_{5/2}$, $^4\Delta_{7/2}$
$Hg_2(^3\Sigma_u)+Br(^2P_u)$	$^2A'+2^2A''$	$^2\Sigma^+_{1/2}$, $^4\Sigma^+_{3/2}$, $^2\Pi_{3/2}$
	$^4A'+2^4A''$	$^4\Pi_{3/2}$
$Hg(^1S_0)+HgBr(^2\Sigma^+)$	$^2A'$	$^2\Sigma^+_{1/2}$
$Hg(^1S_0)+HgBr(^2\Pi)$	$^2A'+^2A''$	$^2\Pi_{3/2}$
$Hg_2(^1\Sigma^+_g)+Br(^2P_u)$	$2^2A'+^2A''$	$^2\Sigma^+_{1/2}$, $^2\Pi_{3/2}$

FIG. (IV-B1). Correlation diagram in (L,S) coupling connecting the reactants $Hg(^3P)$ and $HgBr(^2\Sigma^+)$ to various possible products. In this diagram, the correlation is assumed to go through a HgBrHg intermediate of C_s symmetry.

(IV-B1,B2) show the correlation diagrams in (L,S) coupling. Only those surfaces which directly correlate the reactants to products are drawn. For the complete list of surfaces refer to Table (IV-B1). The "lines" in Figs. (IV-B1,B2) are assigned by connecting reactants to products through mutual surfaces, starting with the product which has the lowest energy.

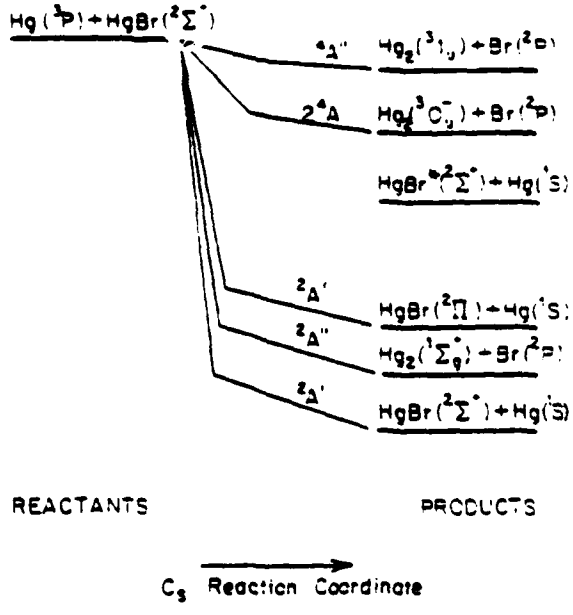

(L,S) Coupling

In the above discussion the interaction of Hg with HgBr utilized (L,S) coupling, this means that the states of Hg, HgBr and HgBrHg are connected such that S is assumed to be precessing about Λ and L.S coupling is small. If the (L.S) interaction term is large the E field in the internuclear axis may not be sufficient enough to cause independent space quantization of L and S with the internuclear components Λ and Σ. The result of L and S form J_a and this precesems about the axis with component Ω. In such cases Λ and Σ are not defined and only Ω retains its meaning as the electronic angular momenta about the axis. To incorporate large spin-orbit interaction in correlation diagrams, the spin states of the species also need to be considered. A first

FIG. (IV-B2). Correlation diagram in (L,S) coupling connecting the reactants Hg(^{3}P) and HgBr($^2\Sigma^+$) to various possible products. In this diagram, the correlation is assumed to go through a HgBrHg intermediate of $C_{\infty v}$ symmetry.

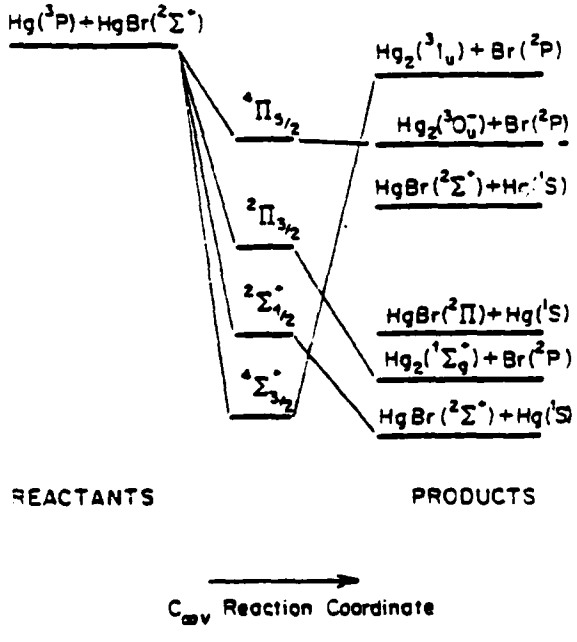

approximation, for not too large spin-orbit interaction is to multiply the orbital eigenfunction with a spin function which has a coordinate system that is fixed on the particular molecule. Unlike space fixed functions which are totally symmetric, such molecule-fixed spin functions are affected by symmetry operations. So one needs to first establish the species of the spin function for various S values for all the important point groups. Herzberg has tabulated this for most S values (Herzberg III, Appendix II, Table 56). To determine the total electronic eigenfunction, one forms direct products of the species of the spin function and the species of the orbital function. Consider again the example of the reaction of equation (B1), assuming large spin-orbit interaction and a nonlinear intermediate (HgBrHg) of C_s symmetry. The parenthetical notes refer the reader to appropriate tables in Herzberg III.

(a) Hg(^3P_u) --> S=1, L=1

resolve L and S into C_s symmetry

P_u	--> 2A'+A"	(App. IV, Table 58)
S	--> A'+2A"	(App. II, Table 56)
^3P_u	--> S x P_u	
	--> (A'+2A")x(2A'+A")	
	--> 5A"+4A'	(App. III, Table 57)

(b) HgBr($^2\Sigma^+$) --> S=1/2, L=0

Σ^+	--> A'	(App. IV, Table 59)
S	--> $E_{1/2}$	(App. II, Table 56)
$^2\Sigma^+$	--> S x Σ^+	
	--> $E_{1/2}$ x A'	
	--> $E_{1/2}$	(App. III, Table 57)

(c) Hg($^1S_0$) --> S=0, L=0

S_g	--> A'	(App. IV, Table 58)
S	--> A'	App. II, Table 56)
$^1S_0$	--> S x S_g	
	--> A' x A'	
	--> A'	(App. III, Table 57)

Having now established the symmetry group of the total electronic eigenfunction, one can correlate the products and the reactants to form a nonlinear intermediate HgBrHg in C_s symmetry.

Reactants:	^3P_u x $^2\Sigma^+$	--> (5A"+4A')x($E_{1/2}$)
		--> 9$E_{1/2}$
Products:	^1S_g x $^2\Sigma^+$	--> A' x $E_{1/2}$
		--> $E_{1/2}$

Baring curve crossing, one can say that the reactants of Eq. (B1) correlate to product species through a single $E_{1/2}$ surface, with the stipulation that the intermediate complex is of point group C_s. In Table

(IV-82) the important product/reactant interaction pairs are tabulated. they are correlated to form an intermediate either in C_s or $C_{\infty v}$ symmetry. Figs. (IV-5,6) in the chapter text show the correlation diagrams in (J,Ω) coupling. Again only those surfaces which directly correlate the reactants to products are drawn. Table (IV-82) contains the complete list of surfaces with the assignment of surfaces being the same as in (L,S) coupling.

TABLE (IV-82). Correlation of various interaction pair to form the intermediate HgBrHg either in C_s or $C_{\infty v}$ symmetry in (J,Ω) coupling.

Process	C_s inter-mediate	$C_{\infty v}$ inter-mediate
$Hg(^3P_2)+HgBr(^2\Sigma^+_{1/2})$	$9E_{1/2}$	$4E_{1/2}+3E_{3/2}+E_{5/2}$
$Hg^+(^2S_{1/2})+HgBr^-(^1\Sigma^+)$	$E_{1/2}$	$E_{1/2}$
$Hg_2(^3\Pi_u)+Br(^2P)$	$18E_{1/2}$	$5E_{1/2}+4E_{3/2}+3E_{5/2}+3E_{7/2}$
$Hg_2(^3\Sigma_u)+Br(^2P_u)$	$9E_{1/2}$	$5E_{1/2}+2E_{3/2}+E_{5/2}$
$Hg(^1S_0)+HgBr(^2\Sigma^+)$	$E_{1/2}$	$E_{1/2}$
$Hg(^1S_0)+HgBr(^2\Pi)$	$2E_{1/2}$	$E_{1/2}+E_{3/2}$
$Hg_2(^1\Sigma_g^+)+Br(^2P_u)$	$3E_{1/2}$	$2E_{1/2}+E_{3/2}$

References (Chapter IV)

[1] R.J. Donovan, Prog. React. Kinet. 10, 253 (1979).

[2] W.R. Breckenridge, H. Umemoto, Adv. Chem. Phys. The Dynamics of the Excited State, K. Lawley, ed., (in press).

[3] D.L. King, D.W. Setser, Ann. Rev. Phys. Chem. 27, 407 (1976).

[4] A.C. Vikis, D.J. Leroy, Chem. Phys. Lett. 21, 103 (1973).

[5] R. Grice, Ph.D. Thesis, Harvard University (1967).

[6] J. Haya, J. Chem. Phys. 67, 4976 (1977).

[7] N. Djeu, C. Mazza, Chem. Phys. Lett. 46, 172 (1977).

[8] R.W. Waynant, J.G. Eden, Appl. Phys. Lett. 11, 708 (1978).

[9] H. Helvajian, C. Wittig, Opt. Commun. 10, 189 (1979).

[10] G. Herzberg, Molecular Spectra and Molecular Structure, Vol. 1, Spectra of Diatomic Molecules (Van Nostrand, Princeton, 1950).

[11] J.G. Calvert, J.N. Pitts Jr., Photochemistry (John Wiley & Sons, Inc., New York, 1967).

[12] R.J. Cvetanovic', Prog. React. Kinet. 2, 39 (1964).

[13] K. Wieland, Z. Elektrochem. 44, 761 (1960).

[14] R. Weast, ed. Handbook of Chemistry and Physics The Chemical Rubber Co., Cleveland, 1973).

[15] J.L. Spier, Physica 7, 381 (1940).

[16] B.E Wilcomb, R. Burnham, N. Djeu, Chem. Phys. Lett. 75, 239 (1980).

[17] J.E. Velasco, J.H. Kolts, D.W. Setser, J. Chem. Phys. 69, 4357 (1978).

[18] M.J. Bevan, D. Husain, J. Photochem. 4, 51 (1975).

[19] G. Herzberg, Electronic Spectra of Polyatomic Molecules (Van Nostrand, New York, 1966).

[20] R.A. Phaneuf, J. Skonieczny, L. Krause, Phys. Rev. A 8, 2980 (1972).

[21] I.N. Siara, L. Krause, Phys. Rev. A 11, 1810 (1975).

[22] σ_{EXP} is defined as $k/\langle v\rangle$ where k is the quenching rate coefficient and $\langle v\rangle = (8kT/\pi u)^{1/2}$ the average collision velocity at 333 K. σ_{HS} the hard sphere cross section is defined as $\sigma_{HS} = \pi R^2$ where R is the collision radius. The calculations assume $R(Hg(^3P_0)) = 1.7\times10^{-8}$ cm and $R(HgBr(X)) = 2.3\times10^{-8}$ cm.

[23] D.D. Darrish, R.R. Herm, J. Chem. Phys. 51, 5467 (1969).

[24] R. Grice, P.B. Empedocles, J. Chem. Phys. 48, 3352 (1968).

[25]L. Grundel, Ph.D. Thesis, University of California, Berkeley (1975).
[26]W.R. Breckenridge, A.M. Renlund, J. Chem. Phys. 61, 1474 (1978).
[27]S. Baur, E.R. Fisher, F.R. Gilmore, J. Chem. Phys. 51, 4173 (1969).
[28]M. Krauss, W. Stevens, Appl. Phys. Lett. (in press).
[29]R.W. Anderson, D.R. Herschbach, J. Chem. Phys. 62, 2672 (1975).
[30]R.W. Anderson, Ph.D. Thesis, Harvard University (1968).
[31]S.A. Edelstein, P. Davidovits, J. Chem. Phys. 55, 5164 (1971).
[32]L. Krauss, The Excited State in Chemical Physics, J.W. McGowan ed., (John Wiley & Sons, New York, 1975).
[33]D.J. Wren, D.W. Setser, J. Chem. Phys. 74, 2331 (1981).
[34]A.N. Zaidel', V.K. Prokof'ev, S.M. Raiskii, V.A. Slavnyi, E. Ya. Shreider, Tables of Spectral Lines (IFI/Plenum, New York, 1970).
[35]J. Maya, IEEE. J. Quantum. Electron. QE-15, 579 (1979).
[36]H. Hofmann, S.R. Leone, (unpublished).
[37]M.A.A. Clyne, M.C. Heaven, J.C.S. Faraday II 74, 1192 (1978).

[38]M.A.A. Clyne, M.C. Heaven, S.J. Davis, J.C.S. Faraday II 76, 961 (1980).
[39]R.G. Aickin, N.S. Bayliss, Trans. Faraday Soc. 34, 1371 (1938).
[40]D.J. Seery, D. Britton, J. Chem. Phys. 68, 2263 (1964).
[41]J.A. Coxon, Molecular Spectroscopy 1, 177 (1973).
[42]C.P. Hemenway, T.G. Lindeman, J.R. Wiesenfeld, J. Chem. Phys. 70, 3360 (1979).
[43]T.G. Lindeman, J.R. Wiesenfeld, J. Chem. Phys. 70, 2882 (1979).
[44]M.A.A. Clyne, M.C. Heaven, E. Martinez, J.C.S. Faraday II 76, 405 (1980).
[45]Ibid. pg. 177
[46]R.E. Sheler, J. Chem. Phys. 21, 624 (1970).
[47]R.J. Donovan, D. Husain, Chem. Rev. 70, 489 (1970).
[48]M.A. Chowdbery, D. Husain, J. Photochem. 7, 41 (1977) and Refs. cited therein.

CHAPTER V

CONCLUSIONS

In the introduction of this thesis several research areas concerning the mercury halide species were discussed as having technological and scientific importance. Through various experiments, the discussions in Chapters II through IV have provided some insight into those research areas. Though some of the pressing questions have been addressed, an equal if not a greater number have not, and as always is with such experiments, new questions have been raised. In this chapter a few of these questions are presented as ideas for future thought.

The largest source of uncertainty in all the kinetic studies reported in this thesis, has been in not accurately knowing the $HgBr_2$ vapor pressure. Though vapor pressure vs. temperature curves do exist, they do not extend to temperatures lower than 100°C.[1] To extend these vapor pressure curves for pressures near room temperatures, extrapolation techniques using computers

were utilized. It must be mentioned that the numbers obtained from the extrapolation agree well with those mentioned in the current literature. In hindsight, it is of importance and of necessity to have the vapor pressure vs. temperature curves of HgX_2(X=Cl,Br,I) species properly extended to regions near room temperature.

The probability for the production of HgBr radicals via $HgBr_2$ photolysis at 193 nm has been measured and is known quite well (Q.E.= 1.0 for forming HgBr(B)).[2-3] However, there has not been a concerted effort to analyze the photolysis products at other wavelengths in the UV. Based on energetics and absorption features it is postulated which products should exist,[4] but one does not know the various photolysis channels as a function of wavelength. For instance, it will be of importance to know whether $HgBr_2$ dissociates to HgBr(X)+Br or Hg+Br+Br for excitations < 50,000 cm^{-1}. Such processes will influence dramatically the number and character of the radical species whose kinetic behavior affect laser performance. Also of importance to the HgBr(B→X) laser is the prerequisite that the laser operate over a great many shots. Therefore recombination processes of the mercury bromide species need to be understood.

Currently working HgBr(B-->X) lasers in sealed systems reach their half power levels after 10^6 shots.[5] It has been assumed that recombination rates are relatively fast to keep the parent species from being removed via contaminating reactions. But to optimize the HgBr(B-->X) laser will require a more thorough understanding of the recombination process.

In the experiments of Chapter IV it was observed that the reactive scattering of metastable Hg atoms with HgBr(X) and Br(^{2}P) showed evidence of ion-pair formation. As previously discussed (Chapter IV), the ion-pair would ensue following charge transfer from the excited atom to the respective bromine. The transient Hg^+Br^- ion-pair has the necessary characteristics of forming electronically excited HgBr(B) species. The potential assymtote for the $B^2\Sigma^+_{1/2}$ state of HgBr is known to correlate to the $Hg^+ + Br^-$ pair.[6] It then becomes the task to find a means of stabilizing the newly formed ion-pair. The fact that HgBr(B-->X) chemiluminescence was observed in the experiments of Chapter IV,

$$Hg(6^3P_0)+HgBr(X^2\Sigma^+_{1/2}) \longrightarrow Hg(6^1S_0)+HgBr(B^2\Sigma^+_{1/2}) \quad (1)$$

$$HgBr(B^2\Sigma^+_{1/2}) \longrightarrow HgBr(X^2\Sigma^+_{1/2}) + h\nu \quad (2)$$

says that a fraction of the scattering pair is

inherently being stabilized to form bound HgBr(B) molecules. Perhaps the spectator Hg atom plays this role for the case of Reaction (1). The fraction of molecules being stabilized is expected to be small because of the fact that repulsive potentials curve cross at high energies of the $B^2\Sigma^+_{1/2}$ electronic state. There are several means with which transient species may be stabilized. Collisional deactivation is the most common and efficient. HgBr(B) vibrational spacing at high v' are expected to be small (~100 cm^{-1})[7] and collisional deactivation is expected to be most efficient (Chapter III Appendix C). A drawback of the collisional quenching scheme is the necessity for high buffer gas pressures (~ 1 atm) which may also quench electronic states of the species involved. The situation could improve slightly if the buffer gas used has small crossection for electronic quenching and large polarizabilities, such as Xe (4.0×10^{-24} cm^3) and H_2 (1.76×10^{-24} cm^3).[8] HgBr(B) has a large static dipole moment and via dipole-induced-dipole processes (long range) or charge-induced interaction (shorter range), the quenching crossections could be made larger than gas kinetic. In the case of quenching vibrational states of HgBr(X,v"), the van der Waals interaction seems to play

a role (see Fig. (III- 7 and 8)) as quenching by Xe was more efficient than He. A van der Waals interaction can increase the quenching radius, as for the case of Xe+HgBr(X,v") the calculation shows the quenching radius to be nearly twice the gas kinetic radii.

References (Chapter V)

[1] R. Weast,ed., Handbook of Chemistry and Physics (Chemical Rubber Co., Cleveland, 1973).

[2] B.E. Wilcomb, R. Burnham, N. Djeu, Chem. Phys. Lett. 75, 239 (1980).

[3] J. Maya, IEEE J. Quantum Electron. QE-15, 579 (1979).

[4] J. Maya, J. Chem. Phys. 67, 4976 (1977).

[5] R. Burnham, E.J. Schimetschek, Laser Focus June (1981).

[6] W.R. Wadt, Appl. Phys. Lett. 34, 658 (1979).

[7] K.P. Huber, G. Herzberg, Molecular Spectra and Molecular Structure: Constants of Diatomic Molecules (Van Nostrand, New York, 1979).

[8] A. Dalgarno, Adv. Phys. 2, 281 (1962).

SELECTED BIBLIOGRAPHY

Allison, J. and Zare, R.N., Chem. Phys. 15, 263 (1978).

Benson, S.W., The Foundations of Chemical Kinetics (McGraw-Hill, New York, 1970).

Burnham, R. and Schimetschek, E.J., Laser Focus, June (1980).

Calvert, J.G. and Pitts, J.W., Jr., Photochemistry (John Wiley & Sons, Inc., New York, 1967).

Chong, Nai-Ho and Cool, T.A., J. Quant. Spectrosc. Radiat. Transfer 21, 397 (1979).

Eden, J.G. and Waynant, R.W., Appl. Phys. Lett. 14, 324 (1979).

Frost, A.A. and Pearson, R.G., Kinetics and Mechanism 2nd ed. (John Wiley & Sons, Inc., New York, 1961).

Gaydon, A.G., Spectroscopy and Combustion Theory (Chapman & Hill, London, 1942).

Greig, G., Gunning, H.E., and Strausz, O.P., J. Chem. Phys. 52, 3684 (1970).

Hayashi, S., Mayer, T.M., and Bernstein, R.B., Chem. Phys. Lett. 51, 419 (1978).

Herzberg, G., The Spectra and Structure of Simple Free Radicals (Cornell University Press, Ithaca, 1971).

Huber, K.P. and Herzberg, G., Molecular Spectra and Molecular Structure: Constants of Diatomic Molecules (Van Nostrand, New York, 1979).

Krause, H.F., Johnson, S.G., Datz, S., and Schmidt-Bleek, F.K., Chem. Phys. Lett. 31, 577 (1975).

Mandl, A., Parks, J.H., and Roxlo, C., J. Chem. Phys. 72, 504 (1980).

Maya, J., J. Chem. Phys. 67, 4976 (1977).

Maya, J., IEEE J. Quantum Electron. QE-15, 579 (1979).

Parks, J.H., Appl. Phys. Lett. 31, 192 (1977); 31, 297 (1977).

Pierce, B.O., Wied. Ann. 6, 597 (1879).

Polanyi, T.M., Atomic Reactions (Williams and Norgate, London, 1932).

Rhodes, C.K., ed., Excimer Lasers (Springer-Verlag, Berlin, 1979).

Rosen, B., Spectroscopic Data Relative to Diatomic Molecules (Pergamon Press, New York, 1970).

Roxlo, C. and Mandl, A., J. Chem. Phys. 72, 541 (1980).

Shay, T., Hammati, H, Stermitz, T., and Collins, J.J., J. Chem. Phys. 72, 1635 (1980).

Terenin, A., Z. Phys. 44, 713 (1927).

Thrush, B.A., Chem. Brit. 2, 287 (1966).

Wadt, W.R., J. Chem. Phys. 72, 2469 (1980).

Wadt, W.R., Appl. Phys. Lett. 34, 658 (1979).

Wehrli, M., Helv. Phys. Acta 11, 39 (1938).

Weston, R.E., Jr., and Schwarz, H.A., Chemical Kinetics (Princeton-Hall Inc., New Jersey, 1972).

Wieland, K., Z. Phys. 76, 801 (1932); 77, 157 (1932).

Wieland, K., Helv. Phys. Acta 2, 46 (1929); 14, 420 (1941); Z. Elektrochem. 64, 761 (1960).

Wieland, K., Z. Phys. 76, 801 (1932).


DAT
FILM